SYNTHESIS AND CHARACTERIZATION OF $LiClO_4$ - LiI SOLID ELECTROLYTE SYSTEM

A Thesis Submitted
In Partial fulfilment of the Requirements
for the Degree of
MASTER OF TECHNOLOGY

by
KRISHNA MOHAN DIXIT

to the
MATERIALS SCIENCE PROGRAMME
INDIAN INSTITUTE OF TECHNOLOGY, KANPUR
JANUARY, 1989

MSP-1989-M-DIX-SYN

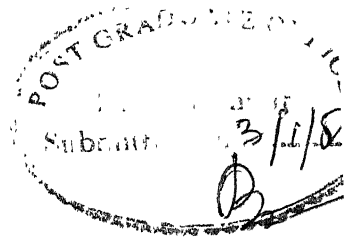

C E R T I F I C A T E

It is certified that this work "SYNTHESIS AND CHARACTERIZATION OF $LiClO_4$-LiI SOLID ELECTROLYTE SYSTEM" by Krishna Mohan Dixit has been carried out under my supervision and that this work has not been submitted elsewhere for a degree.

January, 3, 1989

(K. SHAHI)

Interdisciplinary Programme in
Materials Science
I.I.T. Kanpur

--

ACKNOWLEDGEMENTS

I wish to express my deep sense of gratitude to my reverent guide Dr. K. Shahi for his constant encouragement and invaluable guidance during the course of present investigation.

I would like to thank Mr. J.N. Sharma of the Glass Blowing Lab., IIT Kanpur for his help in this work. The neat typing by Mr. Jawar Singh and careful photocopying by Mr. Vishwanath Singh need special mention. As also the neat drawings by Mr. V.P. Gupta.

My sincere thanks are due to the faculty members of the department who helped me on various occasions.

I sincerely acknowledge the assistance and cooperation provided by my colleagues Ashok Kumar, VPNP Padmanaban, Shiuli Gupta, P. Manoravi and Sujata Chaklanobis. My special thanks a also due to Dr. Y.P. Yadava for his inspiration.

Krishna Mohan Dixit

CONTENTS

--

LIST OF FIGURES

--

LIST OF TABLES

--

ABSTRACT

Solid electrolytes and the related technologies such as high energy density batteries have attracted considerable attention in recent times. The research and development activities have been mainly concerned with developing better and mechanically and electrochemically stable solid electrolytes and producing commercially viable batteries.

Some of the solid electrolytes, such as $RbAg_4I_5$, β-aluminas etc. which were found to exhibit high ionic conductivity and small activation energy failed to lead to commerical batteries either because of economy or poor energy or unstability. For battery application the solid electrolyte should not only be stable and ecomonical but must lead to high energy density. Li^+-based solid electrolytes have now been recognized for their high energy density because of the low equivalent weight of the Li^+ ion and hence a concerted effort is being made worldwide to develop new Li-based solid electrolytes.

$LiClO_4$- organic solvent systems have been widely investigated as potential liquid electrolytes. However it has been least studied as a solid electrolyte. The present work was aimed to investigate the ionic properties of $LiClO_4$ and its potential as a solid state electrolyte.

The system $LiClO_4$ was studied as a single phase and its conductivity ($10^{-8} Ohm^{-1} Cm^{-1}$) at room temperature was found insufficient for battery application. In an effort to improve the conductivity of $LiClO_4$, the system $LiClO_4$-LiI was investigated. The choice of the dopant, I^-, was guided by factors such as the size and the charge of the ion. In addition the conductivity studies on $LiClO_4$-LiI system was expected to substantiate the recent claim that the homovalent dopants can increase the conductivity significantly and also to test the 'lattice loosening' model.

The samples were examined by X-ray Diffraction (XRD) to identify the structures of the starting materials and also the various phases present in the composite system. The DTA was done to identify the phase transitions and melting points of both starting materials and the mixed-systems. Finally the main aim was to investigate the electrical transport behaviour of the starting materials as well as the mixed systems. The conductivity measurements were carried out both in air and in controlled nitrogen atmosphere due to hygroscopic nature of both starting materials.

The XRD results suggest that the starting materials, both $LiClO_4$ and LiI, are in their trihydrate form. Drying these materials at 100°C under moderate vacuum did not affect much, the materials were still trihydrate. Further, it was inferred from the XRD investigations that $LiClO_4$ could dissolve at least upto

8 m/o LiI to form single phase solid solution. Thus the mixed systems containing more LiI than 8 m/o are two-phase mixtures.

The DTA results show thermal events which are attributable either to dehydration or melting of the salt or mixed crystals.

The dc electrical conductivity has been determined for all samples using complex impedance analysis. Both pure $LiClO_4.3H_2O$ and $LiI.3H_2O$ are poor ionic conductors at room temperature. However, the addition of $LiI.3H_2O$ in $LiClO_4.3H_2O$ has been found to increase the conductivity significantly, by a factor of 100 to 1000 depending upon the thermal history and the method used to prepare the samples. $LiClO_4.3H_2O$ + 20 m/o $LiI.3H_2O$ has been found to exhibit the highest conductivity of the order of $10^{-3}Ohm^{-1}Cm^{-1}$ at 110°C.

Finally the electrical conductivity versus temperature studies are reported. The activation energies for ionic transport are calculated and their dependence on the dopant concentration (mol % LiI) is discussed.

CHAPTER 1

INTRODUCTION

1.1 Superionic Conductors :

Superionic conductors or solid electrolytes are a new class of materials in which the electrical conductivity is exceptionally high and the conduction is predominantly due to movement of the ions. Here, ionic conductivity occurs within a well - defined crystalline host whose structure and composition must be maintained for high ionic conductivity to be observed.

The mechanism by which ions diffuse rapidly in these materials are related to those that lead to ionic conductivity in classical ionic solids, such as NaCl, $BaCl_2$ and LiI etc. For these solid crystalline materials, carrier concentration may be defined as the density of defects with reference to the perfect lattice. Each carrier is identically situated and has the same mobility, so that the current due to the ensemble/bulk of ions is a multiple of the single ion current. So in the Arrhenius equation :

$$\sigma = A \exp (- E/ kT)$$

the constants A and E (activation energy) remain the same throughout the range of the temperature, irrespective of composition, for a particular material. This is really different from the amorphous

material, where there are no fixed values of A and E and it's very difficult to assign activation energy for a system. The reason, in amorphous materials, all ions are considered to be potentially mobile/conducting because of open structure.

There are some properties/characteristics common to all superionic conductors (SICs):

(i) a fairly high ionic conductivity (10^{-1} - 10^{-4} $Ohm^{-1}Cm^{-1}$) at moderate temperatures,

(ii) Ions as principal charge/mobile carriers,

(iii) negligible electronic conductivity,

(iv) Crystal bond essentially ionic,

(v) most SICs exhibit a phase transition, when transformed from a low conducting (insulating) state to highly conducting (superionic) state. Few exceptions are like β-alumina, which show an order-disorder transitions,

(vi) the potential energy profiles (i.e. activation energy) along which the mobile ion moves must be low,

(vii) they all owe their conductivities to highly disordered regions in their structures.

These regions may :-

(i) encompass an entire crystal (AgI)

(ii) be restricted to specific internal interfaces (Al_2O_3- dispersed in LiI)

(iii) occur as highly disordered region in the crystal (β-aluminas)

(iv) involve liquid - like diorder of an amorphous (glasses and polymers)

General Conditions for SIC :

There are some conditions to be met in order to have high conducting superionic states. These conditions are:(G.C. Farrington, 1985):

(1) the potentially mobile species must be present as ions and not be trapped in streng covalent bonds,

(2) a population of alternate sites that the ions can potentially occupy and that are not their principal/ regular crystallographic positions must also exist, and ,

(3) the energy to disorder the ions among the larger population of alternate sites and the energy to move the ions among those sites (viz. energy to create a defect) must be low.

In most of the crystals defect energy is quite high, typically 1-2 eV (23- 46 KCal/mole), so the population of defects is small.

What makes the high conductivity solid electrolyte table is that their defect population is very high even at

moderate temperatures, because their defect formation energies are remarkably low. The defect formation energy may be low for one of the several reasons :

(i) Some compounds, such as AgI, Ag_2HgI_4 and $RbAg_4I_5$, undergo specific order/disorder transition that involves a latent heat similar to that of the melting of a solid. This latent heat represents the enthalpy required to disorder ions among the alternate sites in the crystal and therefore to create a large population of defects. At temperatures above the transition, the defect creation enthalpy is essentially zero, i.e., all the ions of one type are available for conduction- a situation similar to that of metals where the so called free electrons contribute to conduction at all temperatures.

(ii) Other compounds such as the beta-aluminas, owe their high conductivities to ionic defects and disorder that are the result of specific compositional non-stoichiometry introduced during their formation.

1.2 Classification of SICs :

There are several ways in which SICs can be classified. These are described in the following sections :

1.2.1 General Classification :

Halogenides :

In this class of SICs, halogen ions (X= Cl,Br,F,I)

constitute the immobile anions and form a static part of the crystal in which they create a large number of voids in which few cations (mobile ions) move and give rise to high ionic conductivity. Halogenide superionic conductors exhibit various forms of Rocksalt structure. Typical examples are :

α-AgI,

$RbAg_4I_5$

Ag_2HgI_4

Beta-Aluminas :

It is a general term that refers to a family of sodium aluminates with closely related structures and chemical properties. The general formula of β - aluminas is

$$Na_2O.\ n\ Al_2O_3\ (\ n = 5 \text{ to } 11\ )$$

The two most important members of this family are the hexagonal (β-alumina) and the rohmbohedral (β - alumina) forms.

β - alumina	$Na_2O.\ 11Al_2O_3$	- Soda excess
β - alumina	$Na_2O.\ 5Al_2O_3$	- Soda deficient

β - aluminas have layered structures with spinel type blocks, such that the two spinel blocks are separated by a loosely packed plane containing Na^+ and O^{-2} ions. Because of the loose packing, space is available for movement of sodium ions leading to high ionic conductivity, as shown by beta- alumina.

Oxide Superionic Conductors :

Oxide solid electrolytes are most commonly used at

elevated temperatures. Useful oxide electrolytes are solid solutions which have the fluorite crystal structures and abnormally high oxygen ion conductivities.

Typical examples :

Stablized Zirconias : $CaO.MO_2$ (M = Zr, Hf, Th, Ce)

$M_2O_3.ZrO_2$ (M = La, Sm, Y, Sc)

1.2.2 Classification of SICs Based on :

(a) Based on Concentration of Defects :

(i) Point Defect Type :

In this class of materials conduction is predominantly due to thermally generated vacancies interstitials. These so called point defects are Schottky or Frenkel type.
Typical examples of materials in this class are :

NaCl	AgI
AgBr	LiI etc.

(ii) Sublattice disorder Type :

Almost all important SICs belong to this category Here the immobile ions (always bigger in size, and in most cases its anions) form a rigid, static part of the lattice (called sublattice) while the smaller conducting ions are distributed hemogeneously over a relatively large number of interstitials (tetrahedral/ octahedral) sites. The result is very high conductivity produced by conducting ion.

Typical examples are :

α-AgI	Beta - aluminas
Rb Ag_4I_5	Li_2SO_4
Li_2S	Li_3N and others.

(b) Type of Conducting Species :

(i) Cation Conductors :

In this class of materials the cations constitute the mobile charge carriers while anions are immobile and contribute to the static part of crystal. So the conductivity is cationic. Typical examples are :

AgI	LiI
CuI	Li_2SO_4
Na_2S	Beta - aluminas
$LiClO_4$	$RbAg_4I_5$ etc.

(ii) Anion Conductors :

There are also SICs where anions are mobile charge carriers and hence contribute to high conductivity. Almost all oxide superionic conductors and few special halides exhibit anionic conductivity. Typical examples are :

YF_3	CaF_2
B_2O_3	$PbCl_2$
$CaO.\ ZrO_2$	$BaCl_2$

$ThO_2 . (Y_2O_3)$ PbF_2

ZrO_2 (Y_2O_3) YCl_3 etc.

(c) Type of Phase Transitions :

Most SIC_s exhibit a phase transition, when they get transformed from a low conducting (insulating) state to highly conducting (Superionic) state. The transitions are of different types, not the same for all SIC_s. According to phase transition, one can classify the SIC_s in three classes : (O' Keeffe, 1979).

(i) Type I (First Order Transition) :

There is a well defined first order phase transition from insulating to superionic phase. Such transitions are accompanied by a latent heat similar to the latent heat of melting, and a large change in the conductivity.

In almost all of these Type I SIC_s there is a rearrangement of the immobile- ion sublattice at the superionic phase transition temperature T_c, in addition to the disordering of the mobile ion sublattice. For example in AgI this lattice transformation is as following :

$$\frac{\beta\text{- AgI (hcp)} \quad \text{or} \quad \gamma\text{-AgI (fcc)}}{\text{Low conducting state}} \xrightarrow[\text{Phase transition}]{\text{Type I}} \frac{\alpha\text{-AgI (bcc)}}{\text{Superionic conducting State}}$$

The typical examples of other materials exhibiting Type I phase transition are :

AgI	YF_3
CuI	Bi_2O_3
Ag_2S	$BaCl_2$ etc.

(ii) Type II (Second Order Transition) :

This is a second order transition and is represented by gradual transition from insulating to conducting state. The conductivity transition is gradual saturation, but the specific heat shows a peak around the saturation (like λ - transition), which confirms that these materials undergo a IInd order phase transition. Examples of materials with second order transition are : PbF_2, $CaBr_2$, YCl_3 etc. This class of materials are really few in number.

(iii) Type III (Faraday transition) :

There is an exponential growth in the conductivity without much cooperative behaviour, i.e. non-conducting- conducting transition is spread over a substantial temperature range. This is also called Faraday transition. Here no peak in specific heat is observed. Typical examples of type III materials are :

beta - aluminas

Na_2S

Li_4SiO_4, etc.

and many others having the fluorite structure (CaF_2, BaF_2, SrF_2,

$SrCl_2$ etc.

(d) Structure :

Structurally, superionic solids can be classified into four categories mentioned below :

(i) Rock Salt Structure :

Halogenides especially LiX belong to this category. Here large ionic randius of the halide ions (x^-) creates a lattice which gives small cations (Li^+) enough space for thermal diffusion. Defects in LiX are generally of Schottky type, and ionic conductivity is isotropic (i.e. no preferred diffusion directions). Cations are mobile species and are octahedrally coordinated. Typical examples are :

LiI, AgI, LiBr etc.

(ii) Fluorite Structure :

It is a face-centred cubic arrangement of cations with anions as mobile species. The cations constitute the static part of the crystal.

	anions :	tetrahedral sites
Cations	Metal ions :	Octahedral sites (surrounded by 8 oxygen ion)

Fluorite (CaF_2) structure has a large number of Octahedral Voids . Thus this structure is a rather 'open' one and rapid ion diffusion might be expected. Typical examples of materials of this class are :

$CaO.ZrO_2$	ZrO_2 (Y_2O_3)
ThO_2 (Y_2O_3)	ZrO_2 (MgO) etc.

(iii) Anti-Fluorite Structure :

Here structure is similar to the fluorite, but the positions of cations and canions get reversed.

Cations : tetrahedral Coordination

anions (O^{2-}) : Octahedral coordination.

Here, conduction is due to cation mechanism, with large amount of cation vacancies in anti-fluorite type structure. Examples of material with anti-fluorite structure are :

ThO_2	Li_2S
ZrO_2	Li_2O etc.

Li_2O structure can be varied by substituting with M^{3+} (M = Al, Ga, Fe and Te) to get materials of the form $Li_5M^{3+}O_4$ (e.g. Li_5AlO_4) which form a superstructure to Li_2O structure.

(iv) Layer Structure :

In this class of materials, there are close packed layers and between two close packed layers a loosly packed plane which is conducting plane containing mobile cations exists. Most prominent members of this class are :

beta - aluminas and

Li_3N, etc.

In β - aluminas, blocks of Al^{3+} and O^{2-} are packed in a similar fashion as the packing in spinel, $MgAl_2O_4$, where Al^{3+} ions occupy the octahedral sites as well as tetrahedral sites (those occupied by Mg^{2+} ion in spinel). The spinel type blocks are separated by a loosely packed plane containing Na^+ and O^{2-}. The layer structure of Li_3N is shown in Fig. 1.1.

1.3 Conduction Mechanism in SIC_s :

1.3.1 Classical Hopping :

In almost perfect crystals, the diffusion of ions takes place in the form of hopping. That is, ions spend most of their time in their respective potential wells and the dwell time of ions in the potential wells is long compared to the hopping time of ions to neighbouring sites.

In FIC_s, the conducting ions are distributed over a large number of available sites (sublattice disorder) and the activation energy of ionic motion is low. This indicates that the potential wells in which the conducting ions are located are shallow. This situation also makes the attempt frequency low.

1.3.2 Cooperative Motions of Ions :

Although the hopping model is able to explain the ionic conductivity of some classical solids like NaCl, $BaCl_2$ etc. it's

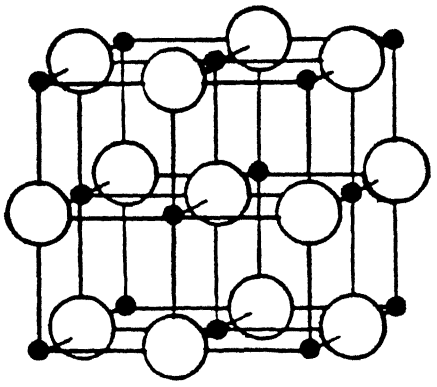

(a) Rocksalt structure

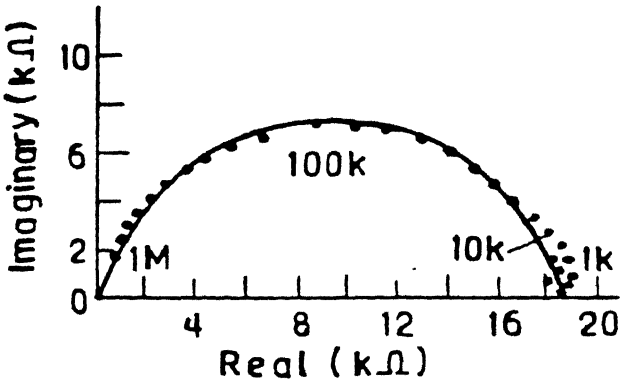

(b) Impedance spectrum

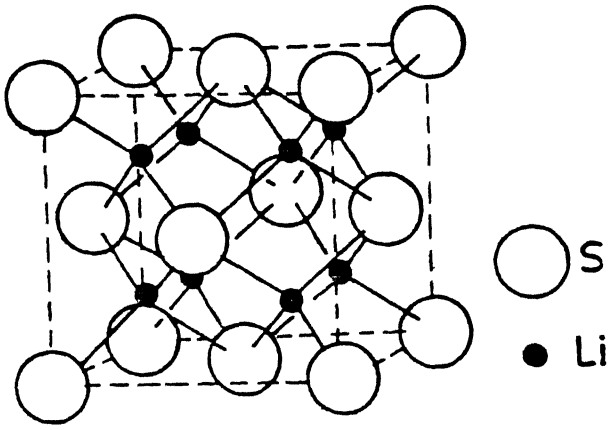

c) Antifluorite structure

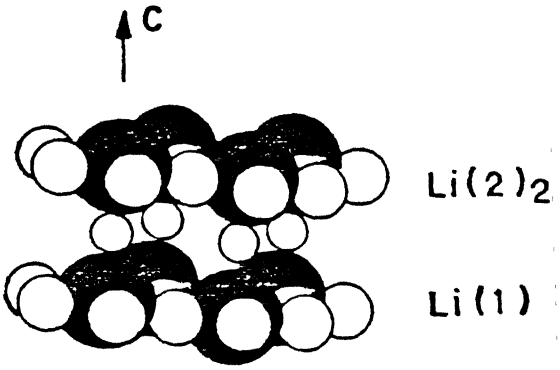

(d) Li_3N Structure

FIG. 1-1

not completely able to explain the high ionic conductivity of extremely fast ionic conductors. Here 'cooperative motions' are much helpful.

(a) Interstitialcy :

It is one of the most commonly known cooperative motions of ions in diffusion. Here two ions, the one on an interstial stite and other on an adjacent regular site, cooperate in such a way that the interstitial ion replaces the ion on the regular site, while forcing the regular ion into an adjacent interstitial site.

(b) Caterpillar Mechanism :

This is based on vacancy mechanism and involves a larger number of ions. In this model a row of ions moves cooperatively by one atomic distance each through a vacancy so that, as a result the vacancy moves a long distance nd, where n is the number of ions involved in the row, and d is the atomic distance. Such a cooperative motion called the 'Caterpillar mechanism' has distinct advantage of increasing the jump distance if it occurs in a straight line as shown in Fig. 1.2 (a).

(c) Cooperative Motion with Zero Activation Energy :

The above discussed cooperative motion of ions are found especially effective in disordered lattices in reducing the activation energy of motion of the group of ions.

Therefore, in a cooperative motion of ions with a fixed interionic distance, all the ions do not follow the path in phase with the period of the potential.

In the third type of cooperative motion, two ions are on the potential well and other neighbouring ions sit on the top of the potential barrier. If these two ions move keeping the fixed interionic distance, a situation (Fig. 1.2b)arises in which one ion is moving upto the potential barrier while the other ion is moving downward to the hill. As a result, the height of the potential barrier for cooperative motion is cancelled, as depicted in Fig. 1.2 (b).

A theory utilizing a mechanism similar to the above has been applied to alumina by Wang et. al.(1975). Essential features of this theory are shown in Fig. 1.3. Wang et. al. used Random Walk theory and calculated an expression for jump frequency and hence conductivity as following:

If the concentration of the excess M^+ ions (M = Rb, Ag, Li) which are occupied in anti Beever-Ross (B-R) sites is n/N

where n is number of excess M^+ ions, and,

N is total number of B-R sites

then jump frequency comes out to be,

$$= 2 \nu_0 (1 - n/N) \exp (- \mu_a/kT) \qquad (1.1)$$

where factor 2 is due to in- phase motion of two- ions and ν_0 is vibrational frequency. So,

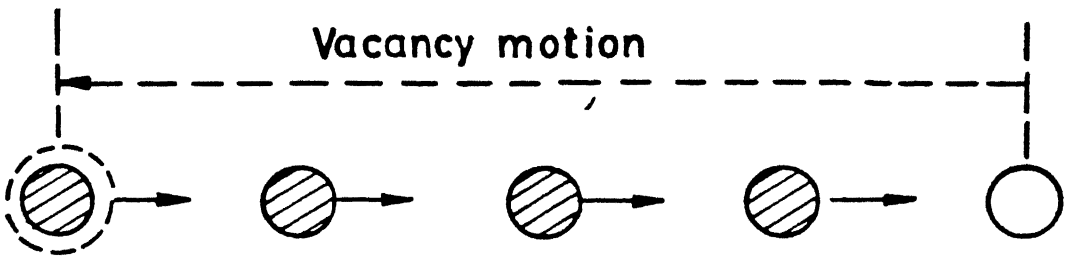

(a)

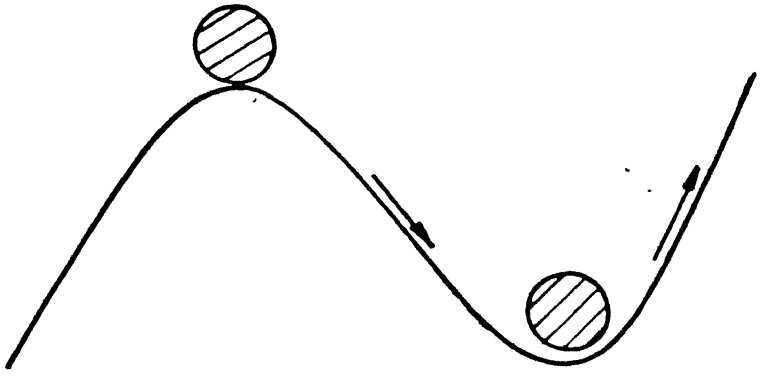

(b)

FIG. 1·2 (a) Caterpillar mechanism of ionic motion

(b) Cooperative motion of two ions with Ea = 0

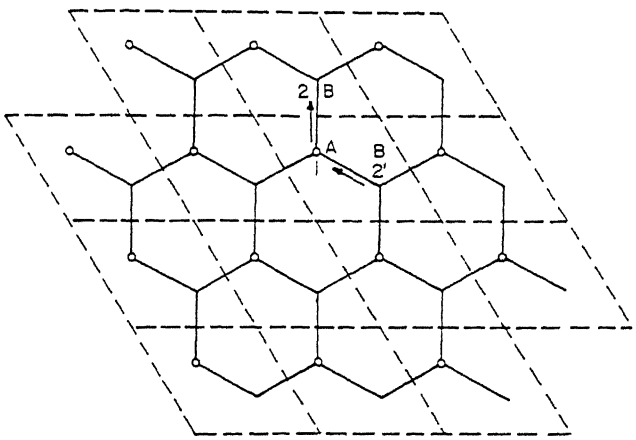

Figure 1.3 The two-dimensional honeycomb lattice indicating the Beevers-Ross Sites (A) and the anti-Beevers-Ross Sites (B) of beta-alumina.

$$\sigma = \sigma_o \exp (-u_a/kT) \qquad (1.2)$$

where $\sigma_o = (\frac{e^2 d^2}{kT}) \nu_o \; n \; (1-n/N)$

d being the interionic separation.

1.3.3 Semiconductor Model (Rice and Roth, 1972):

This model is based on hypothesis that there exist in the ionic conductor an energy gap ϵ_o above which ions of mass M, belonging to the conducting species can be thermally excited from localized ionic states to free-ion-like states in which an ion propagate through the solid with a velocity.

v_m and energy $\epsilon_m = (1/2) M v_m^2$

Then based on Boltzmann transport equation simple expression can be obtained for σ as,

$$\sigma_s = 1/3 \; (Ze^2)/(kT) \; n v_o l_o \exp (-\epsilon_o/kT) \qquad (1.3)$$

By hopping model using Random Walk theory, the expression for σ is

$$\sigma_h = 1/3 \; (Ze^2)/(kT) \; n d^2 \nu_o \exp (-u/kT) \qquad (1.4)$$

where $\nu_o = 1/\tau_o$ is life time of ion in excited state.

So putting in velocity term, one gets.

$\nu_o = 1/l_o \sqrt{2\epsilon_o/M}$ as oscillation frequency. The value obtained, concides with observed Debye frequencies. But this model requires empirically unusual large valve of $l_o \sim 1000A^\circ$ and more than this, the free-ion-like behaviour is questionable.

CHAPTER 2

EXPERIMENTAL DETAILS

2.1 Starting Materials :

(a) $LiClO_4$:

Pure lithium perchlorate (anhydrous) was obtained from 'Alfa Products'. Some of its physical properties are listed below:

Form	:	Polycrystalline colourless small crystals
Mol. wt.	:	106.40
Composition	:	Li-6.52%, Cl-33.33% O-60.15%
Specific gravity	:	2.43
Decomposition and m.p.	:	236°C, decomposition starts at about 400°C and becomes rapid at 430°C yielding lithium chloride and oxygen. (However the m.p. obtained by experiment in our case was around 145 - 146°C which is discussed in later chapter.)
Heat of formation	:	-99.94 KCal/mol at 25°C.
Solubility	:	(W/W) at 0°C, 29.9%, at 25°C, 37.5% at 100°C, 71.5%, and appreciably soluble in alchol, acetone, ether, ethyl acetone.

(b) Lithium Iodide :

Lithium iodide (anhydrous) was also obtained from the 'Alfa Products'. The purity was 98+%. It had a liquid cream colour and was in granual form. However the observed low melting point of this salt led to the suspicion whether it was pure anhydrous LiI or a mixture of anhydrous and hydrated LiI. So LiI as received was investigated by x-ray diffraction. The XRD analysis revealed that the LiI as-received was no longer in anhydrous form but had absorbed water and converted to a large extent into lithium iodide trihydrate. ($LiI.3H_2O$), as discussed in Chapter 3. Some of the physical properties of LiI are listed below:

Form	:	anhydrous, monohydrate, trihydrate, small granuals.
Mol. wt.	:	133.83
Composition	:	I-94.82%, Li 5.18%
Trihydrate	:	White, deliq granuals or fused masses, becomes yellow on exposure to air due to liberation of iodine, m.p. 73°C.
Anhydrous	:	m.p 446°C. Soluble in about 0.5 part water or alchol, freely in amyl alchol or acetone.
Density	:	4.076
Structure	:	Cubic (fcc), Trihydrate (hexagonal)

2.2 Preparation Condition :

The samples were prepared in two different ways. In one case, the starting materials LiI and $LiClO_4$ were used as received.

In the second case the starting materials were predried before mixing the two components. The samples so prepared have been termed" undried" and"predried" samples respectively.

2.2 (a) Undried Samples :

These samples were prepared in two different ways. In the first case the mixture of LiI + $LiClO_4$ was heated to melt and kept there for some time. (30 minutes) followed by cooling to room temperature, grinding and pelletization. In the second case the mixture of $LiClO_4$ and LiI having suitable composition was pressed in form of a pellet and heated for about 9-12 hrs, at an elevated temperature well below the melting point of the mixed salt.

2.2 (b) Predried Samples :

In this case, the starting materials LiI and $LiClO_4$ were dried before mixing them. Both $LiClO_4$ and LiI were dried separately at 120°C under vacuum for 4-5 hrs. The dried samples were stored inside the glove box for further preparations.

2.2 (c) Preparation of Pellets :

The pelletization was done using a H H steel die having inner diameter of 11.2 mm and a hand - operated hydraulic press. The pelletizing pressure was 4 tonnes with 5 minutes for all the samples. The used die is shown in the Figure 2.1.

2.3 Experimental Conditions :

2.3 (a) Open-Air Environment :

The electrical characterization experiments were done in

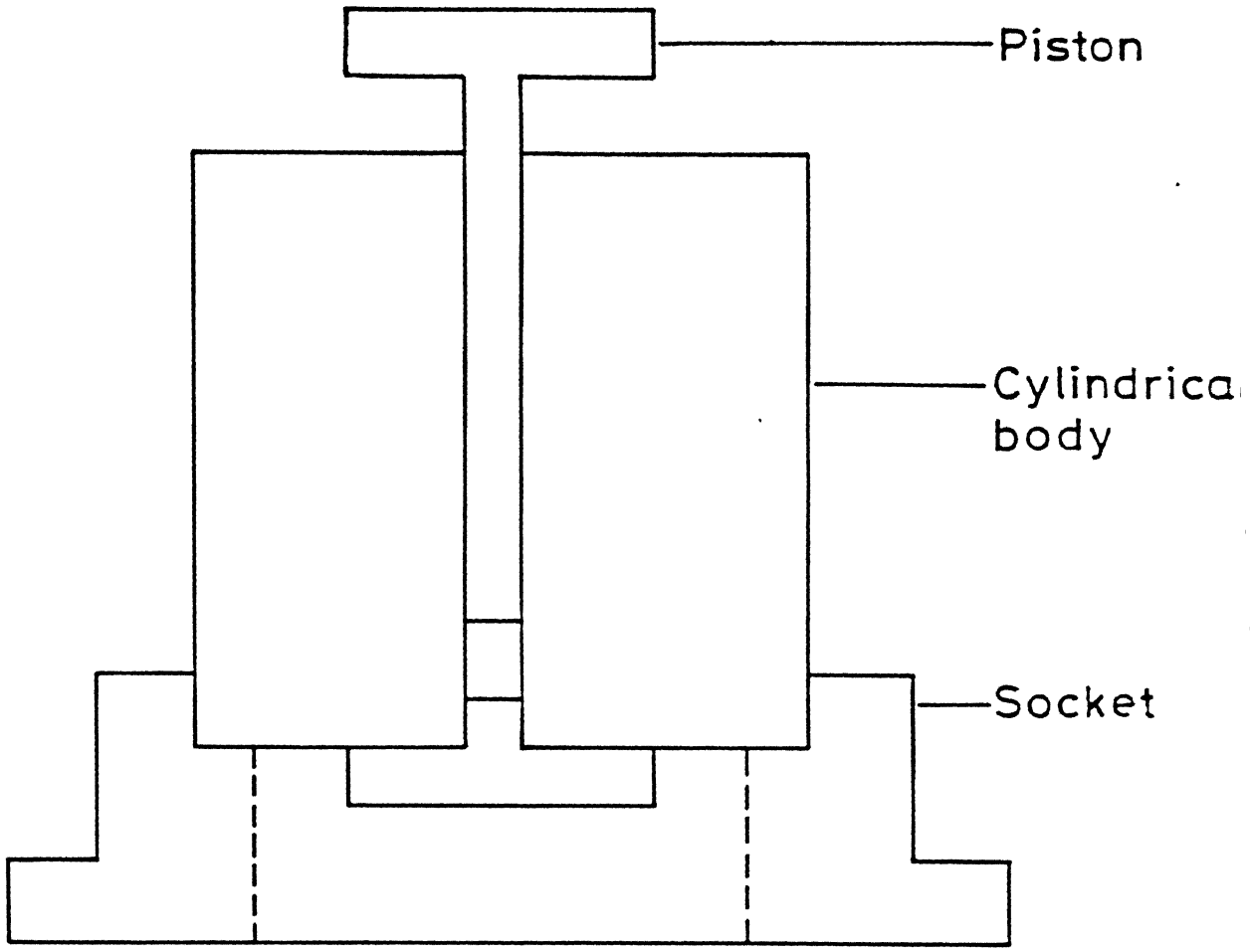

Fig. 2.1 Schematic diagram of stainless steel die .

open ordinary atmosphere as well as in the controlled nitrogen atmosphere, with both oxygen and moisture less than 1 ppm. Initially the experiments were planned and executed in open air environment, but due to hygroscopic nature of both components (especially LiI - which was very much hygroscopic) some unusual results were noticed. To verify them, the experiments were repeated inside the controlled atmosphere glove-box. The results in dry conditions were considerably different from those in used (ambient) conditions. It is quite possible that the moisture present in the air was stimulating some sort of reaction leading to phase transition. These are discussed in detail in the third chapter.

2.3 (b) Controlled in Nitrogen Atmosphere - Glove Box Experiments :

The last phase of experiment involved the use of controlled atmosphere glove box (MECAPLEX - GB-80, Switzerland). The operating conditions of the glove-box are mentioned below:

Inside pressure	Atmospheric
Oxygen Content	5 ppm
Moisture Content	2 ppm
Dew Point (DP)	68°C - 64°C
Inside Temperature	3-5°C above the room temperature

The furnace used inside the glove- box was designed with a special cooling arrangement so as to prevent heat loss inside the glove-box and thus maintain the temperature of the interior near the room temperature. The glove box was also equipped with a digital single pan balance (Mettler - AE 160) which has an accuracy of 10^{-4} g

Experiments on both predried and undried samples were performed inside the gleve box.

2.4 $LiClO_4$- LiI System :

The $LiClO_4$- LiI composite samples were prepared by two ways. The initial set of experiments performed in open air atmosphere (viz. $LiClO_4$ + 10 m/o LiI and $LiClO_4$+ 15m/o) were performed using the method of melt. Later all the mixed samples were prepared by solid state reaction. The separately predried $LiClO_4$ and LiI were physically mixed, grinded and pelletized. The pellets then were sintered for overnight (9-12 hours) at a temperature much below the m.p. of $LiClO_4$ and LiI. The sintering process leads to some solid state reaction making some amount of diffusion of ions (viz I^- here) from the doped material to the host material (i.e I^- replacing some of the ClO_4^- ions in $LiClO_4$). The sintered samples were quite stable with respect to reduced ageing effect and cooling and heating effects in glove-box experiments than open air experiments.

2.5 Electrode Material :

Most of the electrical conductivity measurements were done using stainless steel (ss) electrodes having silver leads spot-welded on to them. The dimensions of steel electrodes were

diameter	:	12.56 mm
Thickness	:	1.94 mm

The stainless steel electrodes were found quite satisfactory when working in the inert atmosphere inside the glove- box. However for experiments carried out in air there was same evidence of slight contamination of electrodes in presence of moisture and oxygen. Therefore one set of measurements on pure $LiClO_4$ sample was performed using platinum electrodes. The conductivity results with ss and platinum electrodes were compared and no marked difference was observed.

2.6 Impedance Measurements :

To obtain the dc conductivity of the samples of various compositions the complex impedance measurements as a function of frequency and temperature were extensively carried out. The various components involved in these measurements are listed :

Furnace
Thermocouple
Sample Holder
Temperature Controller
Digital Multimeter (DMM)
4274 A LF Impedance Analyzer

For the temperature dependance of the conductivity in air, a Kanthal - wire wound horizontal furnace having the characteristics as shown in Figure 2.2 (A) was used. The maximum temperature the furnace could attain was around 1000°C. The furnace used in side the glove- box was a vertical furnace, also made of Kanthal wire, whose lower end was shielded. The general characteristics of the vertical furnace is shown in Figure 2.2 (B). It has an asy-

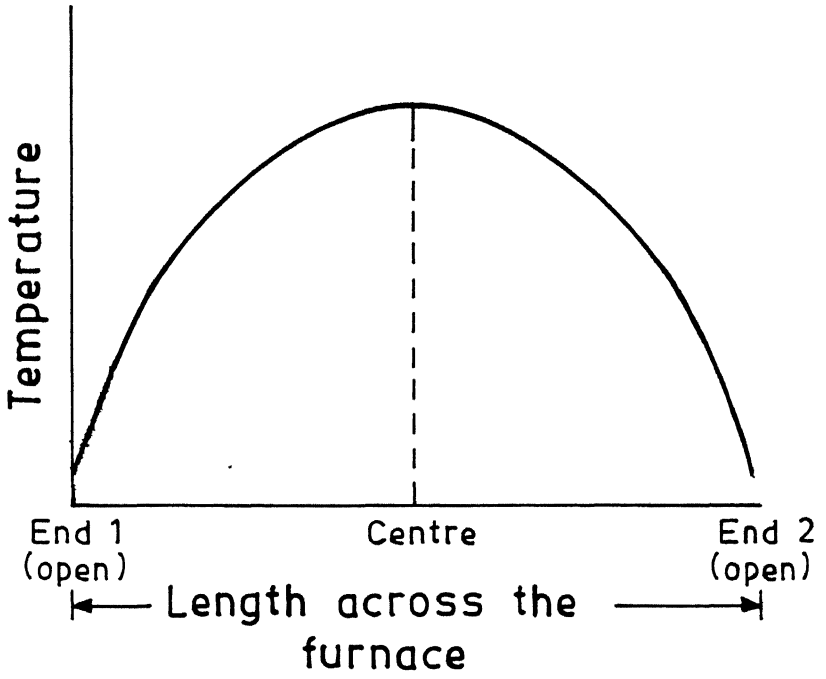

Fig. 2.2(a). The temperature profile of the furnace in horizontal mode.

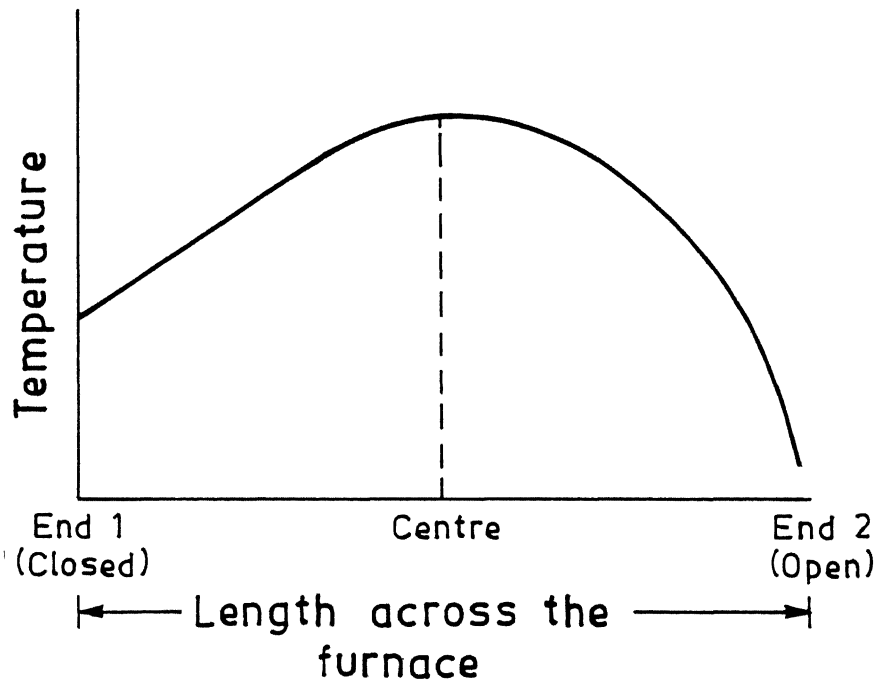

Fig. 2.2(b). The temperature profile of the furnace in vertical mode.

mmetrical characteristic, namely the dissipation at closed end is smaller than that at the open end. A cooling arrangement was also made around the furnace- wall so as to keep the temperature inside the glove- box around the room temperature.

The temperature was measured using chromel- alumel thermocouple (Type K).

The sample holder used for the impedance measurement is shown in the Figure 2.3. It consists of a pair of ss rods of equal dimension. Rods are supported by three lava-discs and a backelite piece at one of the ends. The electrodes and thermocouple are inserted in the sample holder as shown in Figure 2.3,

One of the important requirements of a good sample holder is that the two rods must be parallel throughout so that the axes of spring, quartz tube and lava discs concide with one another. Such a sample holder will ensure a very good contact between the two electrodes and hence will reduce the geometrical capacitance, which is most undesirable in the impedance measurement of ionic and other electrically conducting solids.

2.6.1 Temperature Controller :

Two types of temperature controller were used during this investigation. The experiments conducted in air were performed using an Eurotherm (model no. 021-090-03.276-12.050) temperature controller while the temperature of the furnace inside the glove box was controlled using an Indotherm - 401. In both cases the temperature control was better than $\pm$ 1°C. The thermocouple voltage was measured using a sensitive microvolt DMM Keithley- 177.

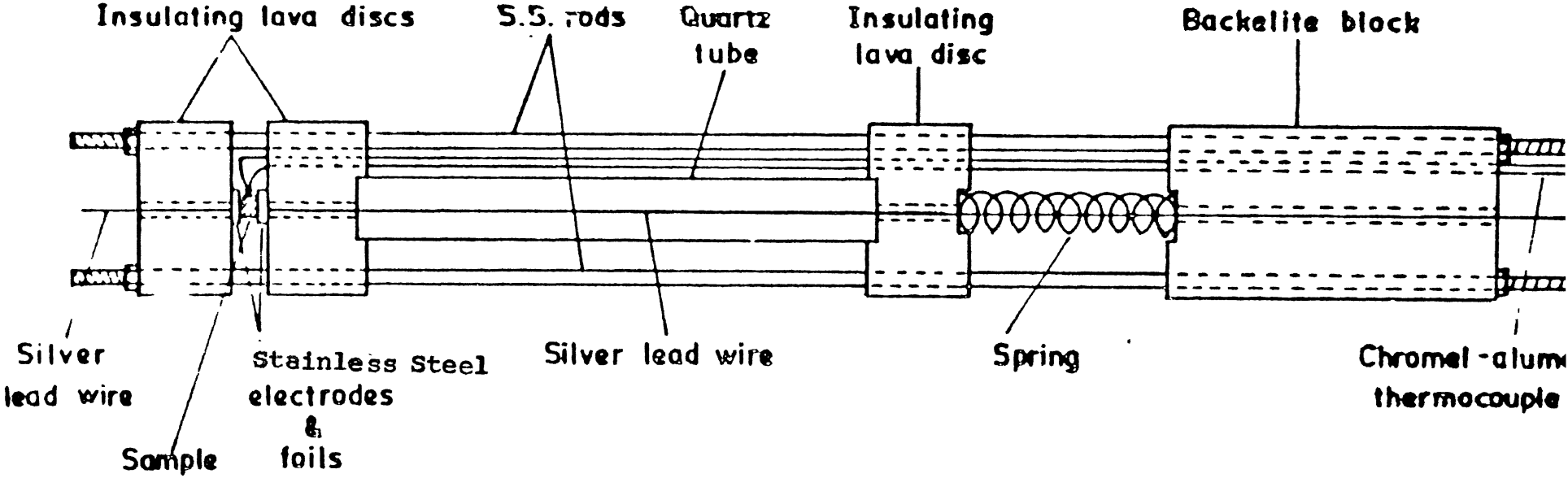

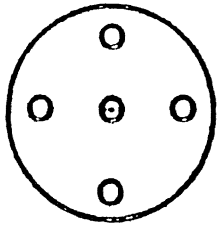

Sectional view of the insulating lava disc

Fig. 2.3 Sample holder for the electrical conductivity measurements.

2.6.2 Multifrequency LCR Meter :

The complex impedance (z) and the phase angle (θ) measurements were carried out using an HP 4274A Multi-Frequency LCR Meter. The test fixture used for external connections was of HP- 16048A type. The LCR meter has 11 discrete frequency steps : 100Hz, 120 Hz, 300Hz, 500Hz, 1 KHz, 3 Khz, 5kHz, 10 kHz, 30 Khz, 50 KHz, 100KHz.

The complex impedance and the phase angle θ were measured at various frequencies and at different temperatures. The same procedure was repeated with samples having various compositions of $LiClO_4$ and LiI.

The circuit used for measurement of complex impedance is shown in Figure 2.4.

2.7 Complex Impedance Analysis :

Complex impedance analysis is the cornerstone of the dc ionic conductivity measurement techniques. A plot is made between resistive ($Z\cos\theta$) and reactive ($Z\sin\theta$) components at various frequencies for a certain temperature. In most of the cases this plot comes out to be a semi-circle with centre lying on the x-axis (in ideal case). The diameter of the semicircle gives the pure dc resistance value at that particular temperature for the system under investigation.

However nature of impedance plot depends on a number of factors which contributes to the total measured impedance.

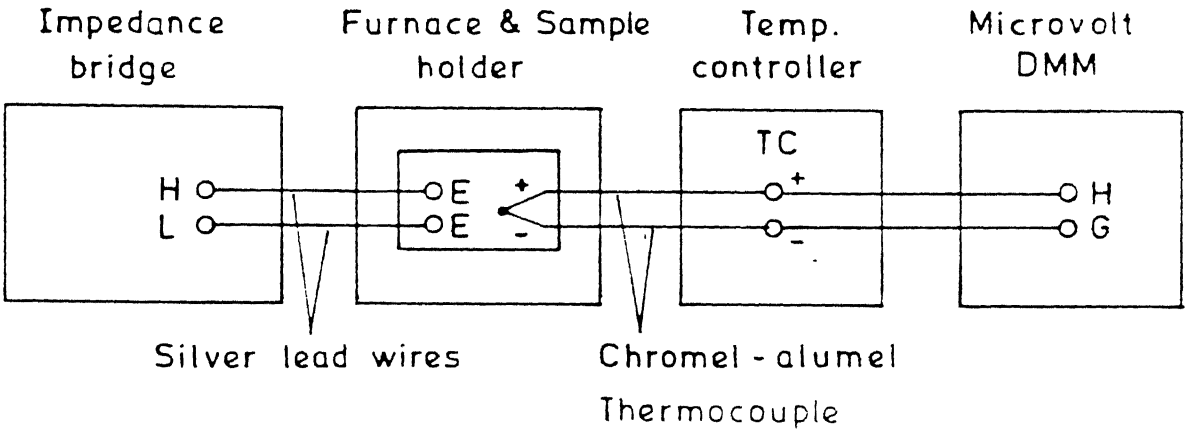

FIG. 2-4 Block diagram connections for electrical conductivity measurements.

1. double layer capacitance C_{dl}
2. geometrical capacitance C_g
3. electrolyte resistance R_e
4. Charge-transfer resistance R_{ct}
5. Warburg impedance W

Three models exist for complex impedance circuit, based on the nature of interface between the solid electrode and the solid electrolyte :

(1) Blocking Electrode/Electrolyte Interface:

A blocking electrode /electrolyte interface means that the electrode does not allow charge transfer to take place across the interface within certain limits of applied voltage for instance, a metal different from silver (e.g. Pt or C) could act as a blocking electrode when anodically polarized in a solid electrolyte which conducts only via Ag+ ion transport (e.g. $RbAg_4I_5$). In such a case the ionic distribution of the electrolyte is perturbed at the interface and a charged double layer is produced between the electrode and the electrolyte.

The equivalent circuit and complex impedance response of metalblocking electrode solid electrolyte interface in the ideal case are shown in Figure 2.5 (A) and 2.5 (B) respectively.

In the ideal case, the circuit gives the complex impedance Z-Z'' plot as shown in Figure 2.5(B). At high frequencies the electrolyte circuit becomes predominent and the semicircle is associated with the geometric capacitance C_g in parallel with the

resistance R_e. At low frequencies the circuit approaches a series combination of C_{dl} and R_e and this gives a vertical line in the complex impedance plane, whose intercept with the real axis Z' gives the value of R_e (Armstrong et.al, 1988).

(2) Interface Between Non-Blocking (Unpolarizable) Electrode Solid Electrolyte :

Non-blocking electrode are unpolarizable electrode, e.g., when Pt is substituted by Ag with $RbAg_4I_5$ Charge transfer can now take place across the interface under anodic polarizations and the equivalent circuit is accordingly modified by the addition of a charge transfer resistance R_{ct}, in parallel with the double layer capacitance C_{dl} (Figure 2.6A) and the complex impedance plot assumes in the simplest case the form of two semicircles (Figure 2.6B).

(3) The Intercalation Electrodes: Warburg Impedance :

An intercalation electrode is generally based on the dichalcogenides of the transition metals. Typical examples are Ti, Ta, Niobium disulphides and diselenides.

Basically these compounds have a two-dimensional layered structure where the basic unit is a sandwich of the three plane, chalcogen-metal-chalcogen(Bonino and Scrosati), with strong covalent bondings. The sandwiches are loosely held together by weak vander Waals forces, so that the various cations such as

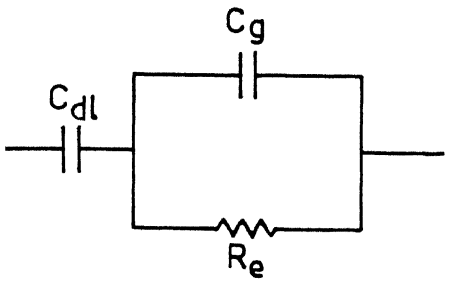

(A)

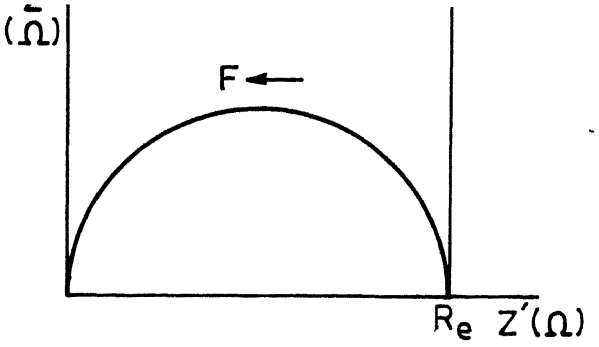

(B)

2.5. Equivalent circuit for the blocking electrodes / solid electrolyte cell assembly (A) and the corresponding frequency response of the impedence (B).

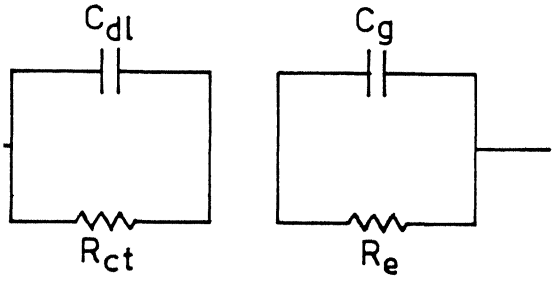

(A)

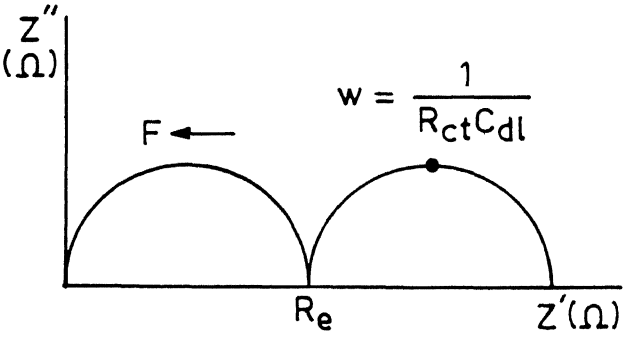

(B)

2.6. Equivalent circuit for the non-blocking electrodes / solid electrolyte cell assembly (A) and the corresponding frequency response of the impedence (B).

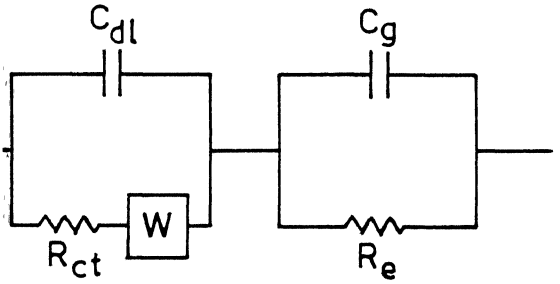

(A)

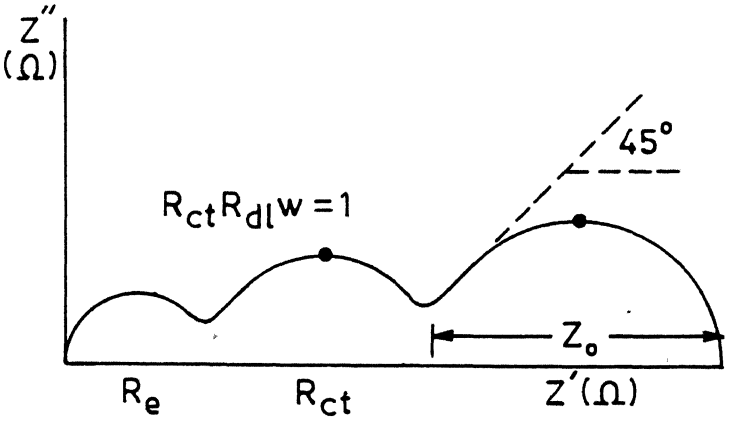

(B)

2.7. Equivalet circuit for the intercalation electrodes : Warburg impeden solid electrolyte cell assembly (A) and the corresponding frequency

Li^+, Ag^+ or Cu^+, can be reversibly intercalated between them producing only an expansion along C-axis with no permanent damage in the host structure. Consequently in the interface between an intercalation electrode and a cation-conducting solid electrolyte, the charge transfer process is accompanied by the diffusion of the intercalated ionic species to and from the bulk of the electrode. Accordingly, the equivalent circuit differs from that of a typical metal electrodes by the addition of a general impedance called the 'Warburg impedance' which represents a kind of resistance to mass transfer [Figure 2.7(A) and 2.7 (B)].

The complex impedance analysis was done during the experiment by PC using a software developed for this purpose [Bhatnagar et. al 1988). In most of the cases the plots obtained between Z' and Z'' were semi-circle or part of a semi -circle.

However in almost all cases at higher temperatures the impedance plots consist of two branches of a curve intersecting on the real-axis. The point of intercept on real axis was taken equal to diameter of semi-circle and the dc-resistance value calculated.

2.8 XRD :

$LiClO_4$, LiI and their mixed crystals were investigated by XRD at room temperature. The material was loaded in powder form and the XRD patterns were recorded as a function of diffraction angle 2θ. Following are the constants used in XRD of all samples:

Wavelength of x-ray radiation	1.546 A° CuK_{α}
Counting/second (CPS)	1 K
Time constant (Tc)	10 sec
Filter	Ni
Scanning speed (SS)	30/min in 2θ
Chart speed (CS)	30 mm/min
Target potential difference/ current	20 mA/30 kV

The objectives of taking XRD was two-fold :

(1) To determine the crystalline state and the form of the two starting materials, $LiClO_4$ and lithium Iodide (LiI). This was achieved by comparing the observed XRD patterns with the standard d values available in ASTM . XRD data. The detailed results of XRD and analysis is mentioned in Chapter III.

(2) The second and important purpose of XRD was to get a knowledge of the state of mixed materials- whether they ($LiClO_4$ and LiI) form a solid solution and if they do, then what is the range of solid solubility. Moreover, XRD pattern can be helpful in identifying the presence of any intermediate compound that may be formed. All these aspects can be used to construct the phase diagram of the $LiClO_4$-LiI system.

2.9 DTA :

The Differential Thermal Analysis (DTA) was carried out for one set of undried samples experimented inside the glove-box. The main purpose of DTA was to identify the possible phase trans-

itions in both pure salts and the mixed-salts, if there is any, and to determine the melting points of both starting materials and those of the mixed systems.

The DTA was carried out using a Linseis- L81/092 with a heating rate of 5°C/min.

However, the m.p. obtained by DTA and those mentioned in the'CRC Handbook of Physics and Chemistry'and'Merck Index' were generally not in agreement. It is discussed in more detailed in the Chapter 3.

--

RESULTS AND DISCUSSION

3.1 XRD :

Some of our initial measurements and other experiments indicated that our lithium perchlorate sample had a much lower melting point than that reported in literature (236°C) for anhydrous $LiClO_4$. It became imperative to ascertain the correct phase and the melting point of the starting material $LiClO_4$. For the latter experiment we chose three different samples.

(i) $LiClO_4$ as supplied by manufacturer
(ii) dried $LiClO_4$ in vacuum for 5 hrs at 120°C and,
(iii) dried material (as above) in pellet form pressed at 4 tonnes.

When the melting point was determined inside the glove box, all the three samples gave the same result, around 145°C.

XRD analysis was done to identify the correct phase of the material. The XRD patterns of as received lithium perchlorate revealed that the material was $LiClO_4.3H_2O$ and not anhydrous $LiClO_4$ as claimed by the manufacturers. The XRD data are given in Table 3.1, which contains all the characteristic peaks of $LiClO_4$-$3H_2O$ as reported in ASTM. Our experiments as well as the standard ASTM have employed CuK_α radiation and Ni as filter. The XRD pattern of $LiClO_3.\ 3H_2O$ is shown in Figure 3.1. $LiClO_4.\ 3H_2O$ has hexagonal structure (a = 7.719 Å, c = 5.455 Å). It is reported to melt at 90°C while the anhydrous one at 230°C. Our melting point and XRD results then suggest that (i) our lithium perchlorate is largely in trihydrate form but contains a small

Table 3.1 XRD Analysis of $LiClO_4.3H_2O$

2θ (degree)		θ (degree)	Sin θ	Calculated $d = \frac{\lambda}{2 \sin \theta}$ A°	d(stnd.) ASTM data	I/I	hkl (hexa gona
13.3	w	6.65	0.1158	6.650	6.69	20	100
21.0	vs	10.50	0.1822	4.227	4.23	100	
23.2	vs	11.60	0.2010	3.830	3.862	75	110
26.7	w	13.35	0.2308	3.330	-	-	-
31.4	vs	15.70	0.2706	2.846	2.850	90	201
32.9	s	16.45	0.2831	2.720	2.726	25	002
35.5	s	17.75	0.3048	2.526	2.528	30	210,1(
39.3	w	19.65	0.3363	2.290	2.292	18	211
47.2	w	23.6	0.4003	1.924	-	-	-
49.2	w	24.6	0.4163	1.850	1.854	10	310,21
52.2	s	26.1	0.4399	1.751	1.756	14	311,1(
57.8	w	28.9	0.4833	1.594	-	-	

(Target)

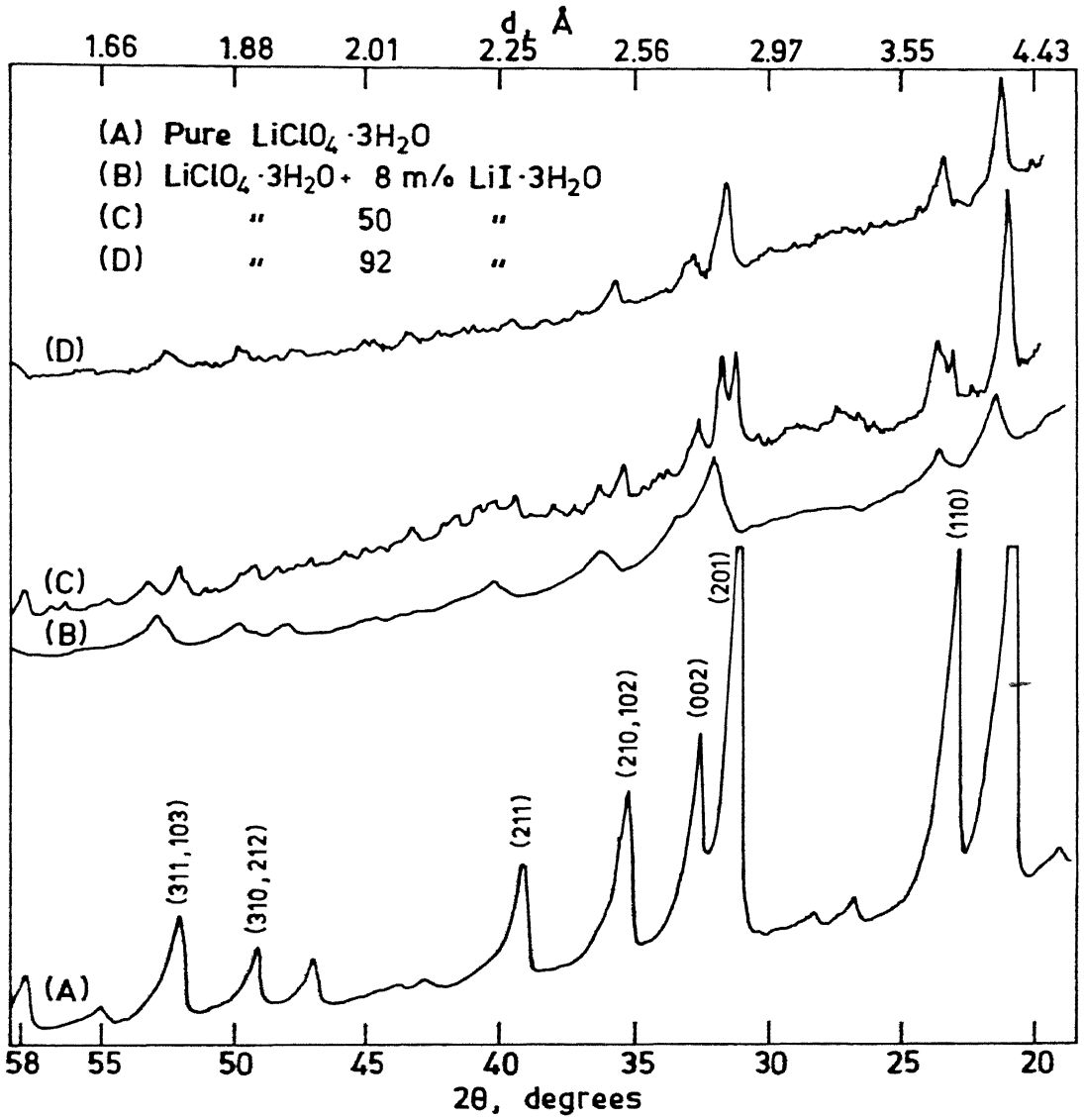

Fig. 3.1. X-ray diffraction patterns (undried samples).

fraction of anhydrous $LiClO_4$ and (ii) drying the material at 120°C for several hours is not enough to make the salt anhydrous, i.e., the dried salt is still $LiClO_4 . 3H_2O$ with perhaps an increased concentration of the anhydrous $LiClO_4$.

3.1.2 Pure LiI :

Almost same problem was faced with LiI also. The melting point of anhydrous LiI is reported to be 446°C, however the LiI as received from the manufacturers appeared to melt at much lower temperature, below 200°C.

The XRD analysis of LiI showed that LiI was no longer in anhydrous form but it had absorbed water and got converted into trihydrate i.e. $LiI . 3H_2O$. The XRD data has been given in Table 3.2. These data when compared with the standard ASTM data clearly establish that the salt is in its trihydrate form ($LiI.3H_2O$). The three characteristic peaks of $LiI.3H_2O$ corresponding to d values of 4.19 A°, 3.74 A°, 2.79 A° are exactly matching with the standard ASTM data. The XRD pattern is shown in Figure 3.2. There are two patterns : one is for LiI dried at 100°C under vacuum and the other for undried LiI. However a comparision of both the patterns suggests that drying of the salt does not make much of a difference and the salt (dried and undried) remains largely in trihydrate form. The fact that some of the peaks present in the undried salt are suppressed or missing in the XRD pattern of the dried salt only indicates that the fraction of the former is somewhat reduced. No further effort was made to obtain anhydrous LiI as the subsequent handling of the material in air will reverse

Table 3.2 XRD Analysis of $LiI.3H_2O$

CuK_α + Ni Filter λ = 1.54 A°

d values (in A°) - Hexagonal					
undried		dried		Stnd. (ASTM)	I/I_1
4.187	vs	4.187	s	4.19	100
3.735	s	3.751	w	3.74	90
2.781	s	2.786	w	2.79	
2.233	w	2.241	vw		
2.207	w	2.209	vw		
1.702	w	1.05	vw		

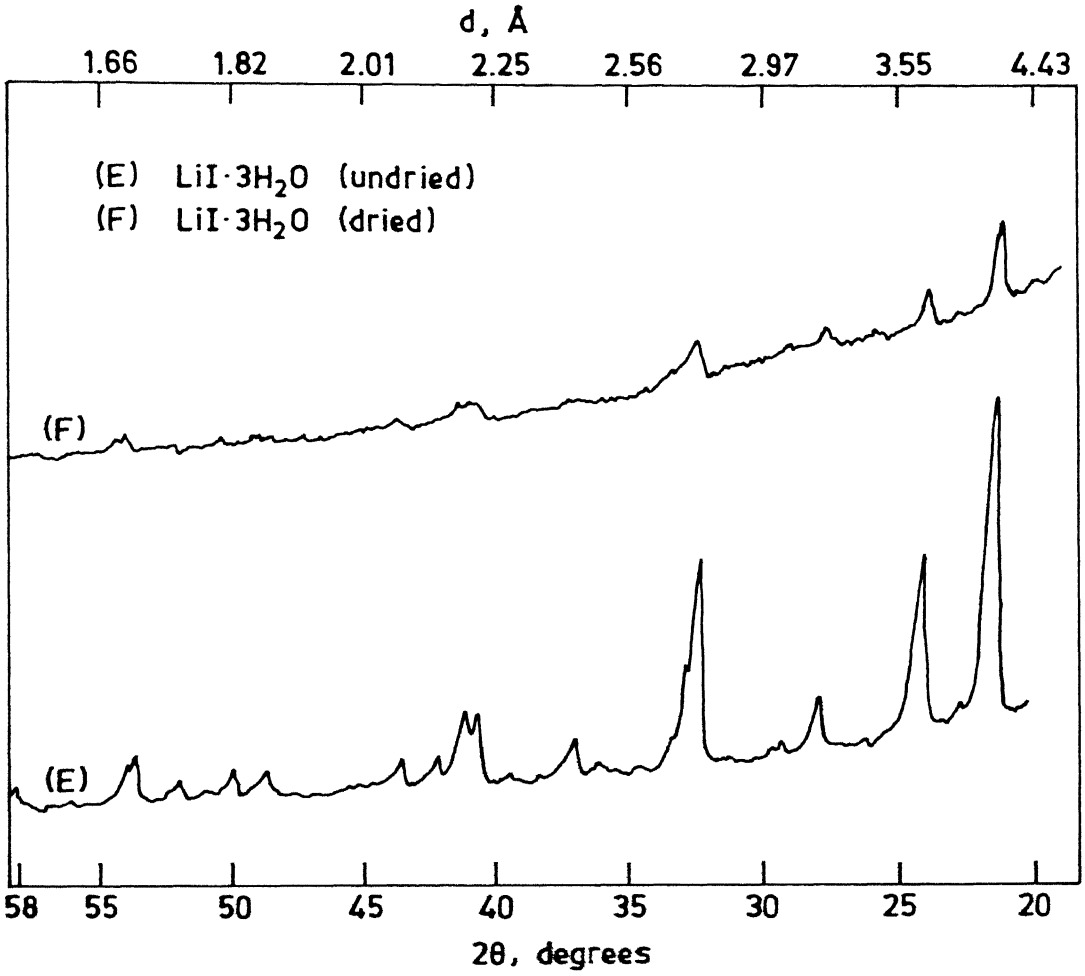

Fig. 3.2. X-ray diffraction patters of $LiI \cdot 3H_2O$.

it to the hydrate form.

Thus both the starting materials, LiI and $LiClO_4$ used in the present investigation were in their trihydrate form even though they were procurred in anhydrous form. The drying at 100°C for several hours did not yield pure anhydrous salts. In fact from the XRD patterns of the dried salts it would seem that the trihydrate form forms the major component in the dried salt as well.

3.1.3 XRD Patterns of $LiClO_4$-LiI Mixed Salts :

The mixed crystals of $LiClO_4.3H_2O$-$LiI.3H_2O$ system were examined by XRD analysis at room temperature. The XRD data summarized in Table 3.4 for the mixed crystals containing 8,20, 40,50,60, and 80 mole % LiI besides the two starting materials. The XRD data of Table 3.3 contain nothing to suggest the existence of any intermediate new phase in this binary system. There is evidence of solid solubility of $LiI.3H_2O$ in $LiClO_4.3H_2O$ and vice versa at the two extremes and mixed phases for intermediate composition ranges. The XRD patterns are shown in Figures 3.1, 3.3 and 3.4.

It is evident from the data of Table 3.3 that the sample containing 8 m/o $LiI.3H_2O$ is a single phase solid solution as there are no lines corresponding to the $LiI.3H_2O$. The effect of the dopant (8 m/o $LiI.3H_2O$) is to shift almost all the peaks a little towards lower 2θ values. This means the effect of I^- doping is to increase the lattice parameters of the hexagonal $LiClO_4.3H_2O$ which

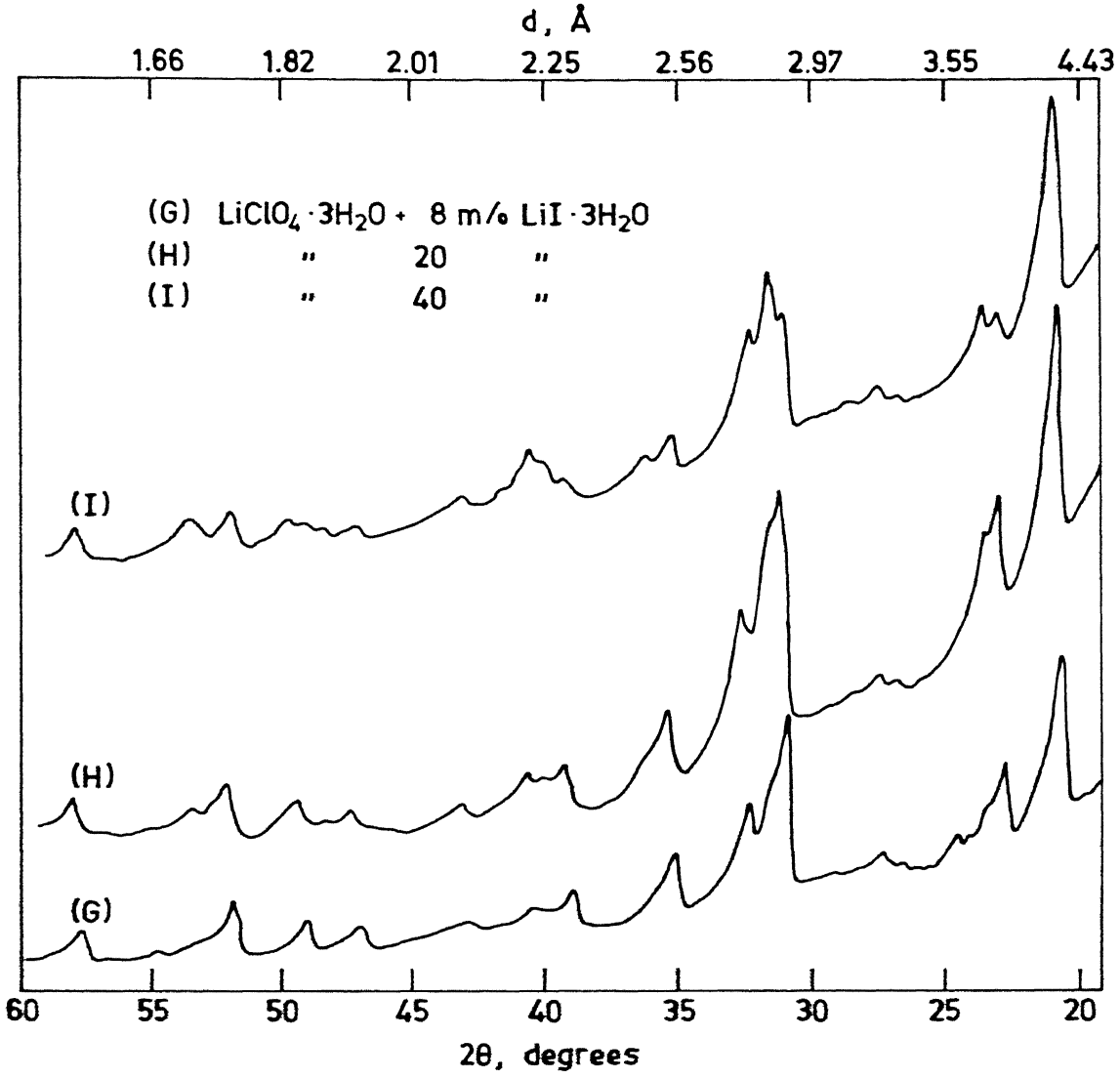

Fig. 3.3. X-ray diffraction patterns (dried samples).

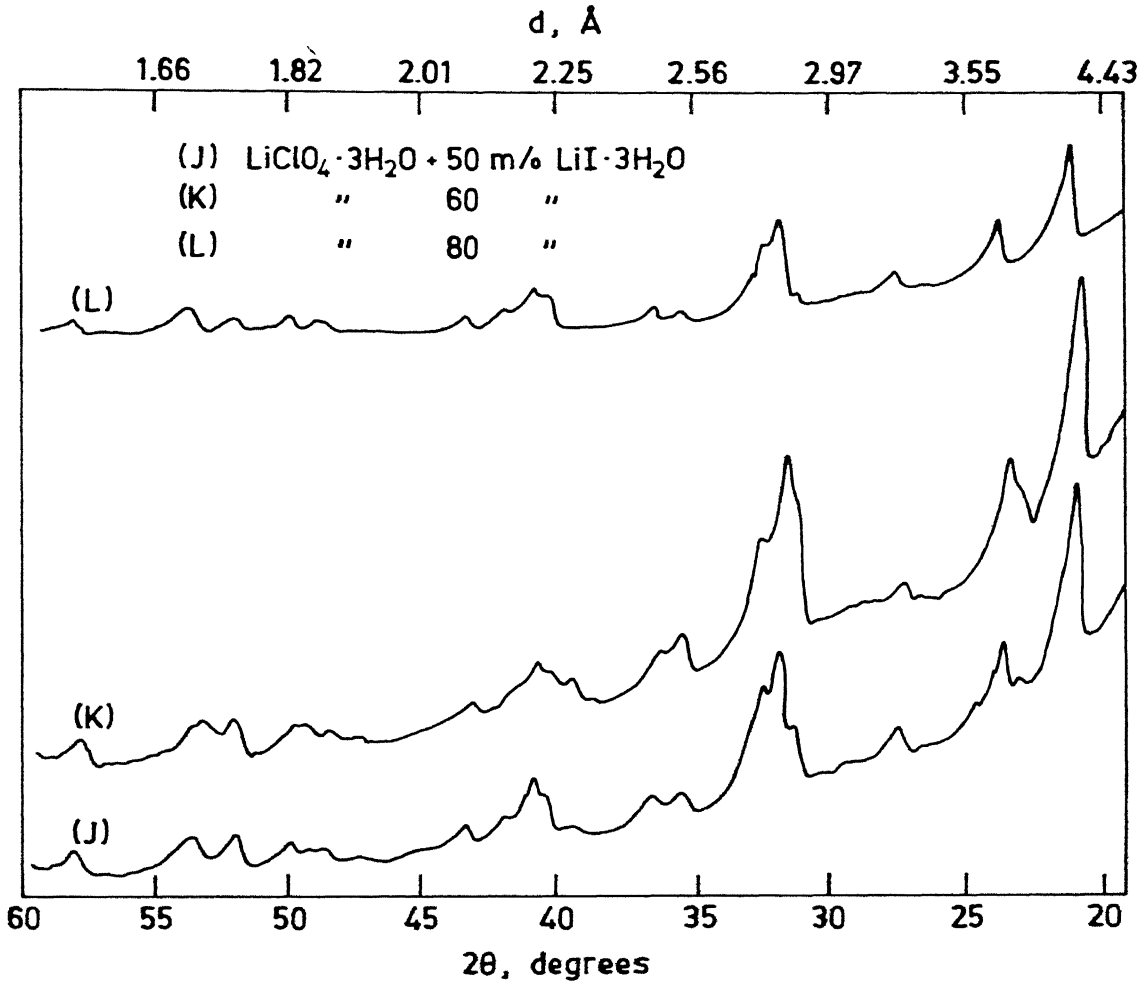

Fig. 3.4. X-ray diffraction pattrns (dried samples).

is consistent in view of their sizes, I^- (2.16 Å) and ClO_4^- (2 Å). The sample with 20 m/o $LiI-3H_2O$ shows two additional peaks corresponding to $LiI.3H_2O$ at 2θ values of 23.6 (s) and 43.3 (vw). For $LiClO_4$ containing 40 m/o $LiI.3H_2O$, there are four additional peaks corresponding to $LiI.3H_2O$. However the samples containing higher amounts of $LiI.3H_2O$, a triplet peak pattern is obtained around 2θ range of 31.4 to 32.85°.

For equimolar mixture = (50 m/o each) the triplet is quite pronounced but one of the peaks of the triplet (2θ = 31.55°) becomes weak and subsequently disappears for yet higher concentrations of $LiI.3H_2O$. For $LiI.3H_2O$ rich compositions, the additional peaks correspond to those of $LiClO_4.3H_2O$.

In 60 m/o $LiI.3H_2O$ sample the dominating phase is expectedly $LiI.3H_2O$ itself. The addition of $LiClO_4.3H_2O$ only modifies the patterns of $LiI.3H_2O$ with additional peaks having 2θ values 31.9 (vs), 32.85 (s), 35.7 (w), 39.5 (vw), 52.15 (w), 57.8(w) correspond to $LiClO_4.3H_2O$.

In 80 m/o $LiI.3H_2O$ specimen, a couple of peaks of $LiClO_4.3H_2O$ still appear, viz, at 2θ = 32.7 (s) and 35.7 (vw), all others belong to $LiI.3H_2O$.

The solid solubility of $LiI.3H_2O$ in $LiClO_4.3H_2O$ at room temperature appears to be anywhere between 8 and 20 m/o. The solubility of $LiClO_4.3H_2O$ in $LiI.3H_2O$ is relatively small.

Table 3.3 XRD Analysis of $LiClO_4$- LiI System : 2θ values corresponding to various observed peaks.

MOLE PERCENT OF $LiI.3H_2O$ IN $LiClO_4.3H_2O$															
0		8		20		40		50		60		80		100	
13.3	w														
21.0	vs	20.9	vs	21.1	vs	21.2	vs	21.3	vs	21.15	vs	21.2	s	21.2	vs
23.2	vs	22.9	s	23.15	s	23.65	w	23.8	w	23.6	s	23.75	w	23.8	s
26.7	w	-	-	23.6	s-							27.6	vw	27.6	w
						27.5	vw	27.8	vw	27.4	w	-	-	-	
31.4	vs	31.3	vs	31.5	vs	31.4	s	31.55	w_+	31.9	vs_+	32.1	s	32.15	s
32.9	s	32.75	s	32.95	s	32.0	vs-	32.15	vs	32.85	s_+	-		-	
-		-		-		32.10	s	32.75	s_+			32.7	s_+	32.65	w
35.5	s	35.45	w	35.7	w	35.6	w	35.65	w_+	35.7	w_+	35.7	vw_+	36.7	vw
39.3	s	40.25	vw	39.5	vw	40.3	vw-	40.3	vw	39.5	vw_+	36.8	vw	40.35	w
-		-		43.3	vw-	40.7	w-	40.85	w	40.2	vw	40.35	vw	40.85	w
47.2	w	47.1	vw	-		-		-		40.7	w	40.5	w	40.85	vw
49.2	w	49.2	vw	-		-		-		43.15	vw	40.35	vw	43.3	vw
52.2	s	52.1	w	52.35	vw	52.2	w	52.2	w_+	52.15	w_+	50.1	vw	50.1	vw
-		-		-		53.6	vw-	53.8	w	53.45	w	50.1	vw	50.1	vw
57.8	w	57.7	vw	58.05	vw	57.9	w	58.0	w	57.8	w_+	52.2	vw	52.2	vw
63.0	w	-		-		-		-		-		54.0	w	53.8	w
73.7	w	-		-		-		-		-		58.11	vw	58.1	vw

2 θ values - XRD Data (degree)

- denotes additional line corresponding to $LiI.3H_2O$.
+ denotes additional line corresponding to $LiClO_4.3H_2O$.

vs, s and w denote very strong, strong and weak peak respectively.

3.2 Differential Thermal Analysis (DTA) :

DTA was performed with a dual objective: Firstly, to confirm the transitions appearing in the conductivity measurements and secondly, to determine the melting point of both LiI and $LiClO_4$.

The DTA results are summarized in Figure 3.5 and Table 3.4 where DTA data have been tabulated for five different compositions including the two pure starting components $LiClO_4$ and LiI, and remaining three for mixed salts with compositions 8, 50 and 92 m/o $LiI.3H_2O$.

The DTA results suggest that the melting point of $LiClO_4.3H_2O$ is 145°C and that of $LiI.3H_2O$ is 105°C. The meling point (145°C) of the $LiClO_4.3H_2O$ was in good agreement with an independent, direct determination inside the glove box as mentioned in 3.1. However these data are at variance with those reported in 'CRC Handbook of Chemistry and Physics'. It is believed that neither $LiI.3H_2O$ nor $LiClO_4.3H_2O$ can be obtained as a single phase material and the quantity of the second and/or third phases present in them would vary depending upon the history of the samples leading to different melting points. For example, from our XRD results of $LiClO_4.3H_2O$ it is clear that the trihydrate phase is the dominant one but a little higher melting point (145°C) than the reported value of 95°C suggests that some anhydrous form (m.p 236°C) is also present.

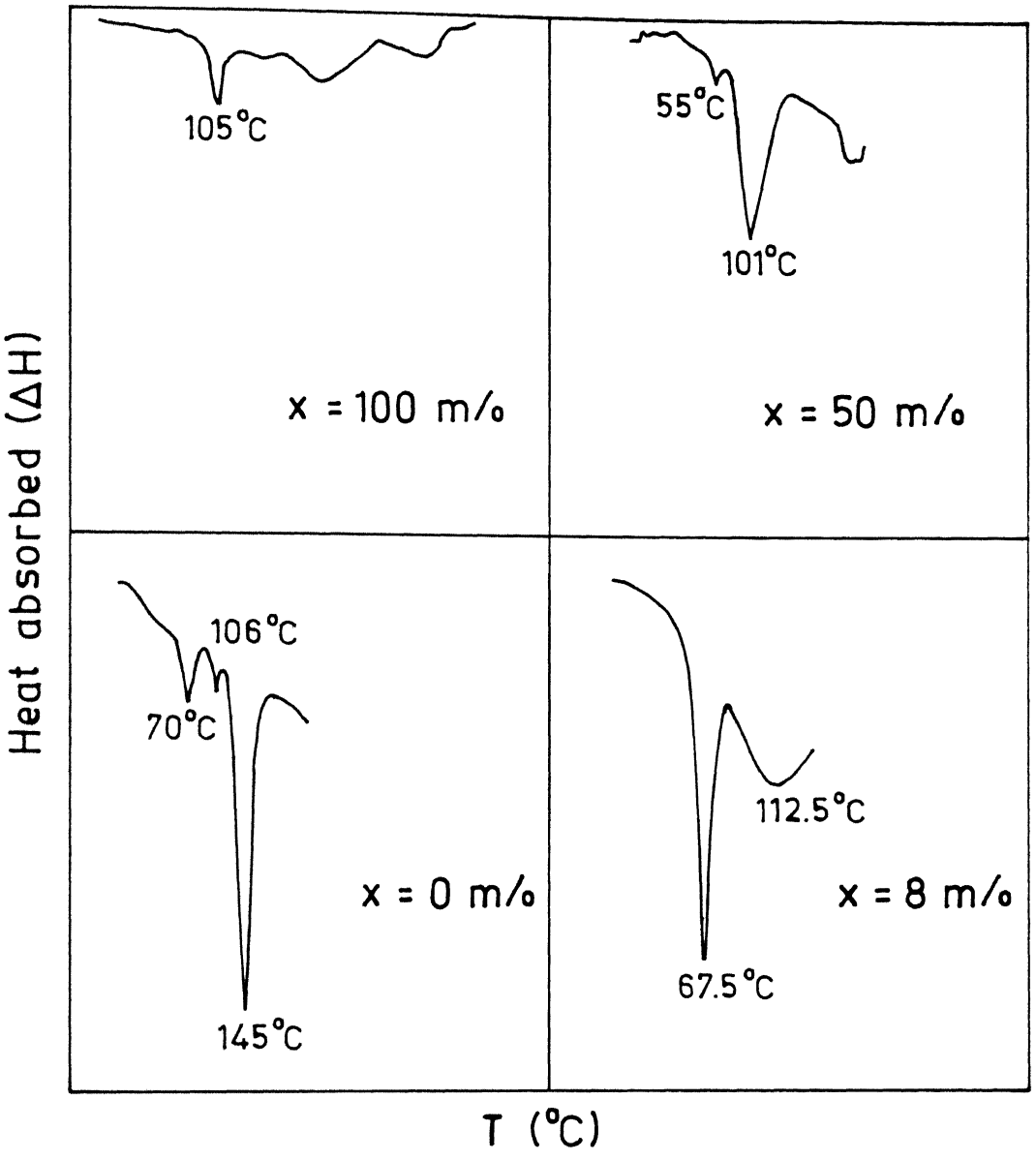

Fig. 3.5. DTA curves of $LiClO_4 \cdot 3H_2O$ + x m/o $LiI \cdot 3H_2O$ (undried) samples.

Table 3.4 Results of DTA for various compositions

System	Transitions (°C)		m.p. (°C)
	I	II	
$LiClO_4.3H_2O$	70	106	145
$LiClO_4$-LiI (8m/o)	-	67.5	112.5
$LiClO_4$-LiI (50m/o)	55	-	101
$LiClO_4$-LiI (92m/o)	-	-	85
$LiI.3H_2O$	-	-	105

The DTA curves shown in Figure 3.5 for $LiClO_4.3H_2O$ exhibits three thermal events at 70,106 and 145°C. The ones at 70° and 106° should be associated with dehydration of the $LiClO_4.3H_2O$ in steps while the third and the sharper one at 145°C corresponds to the melting transition. The melting point of 145°C for $LiClO_4.3H_2O$ was confirmed by direct experiments as well.

As-received LiI was not in the anhydrous form but it had picked up water forming one of the three hydrated salts. The XRD and DTA both confirmed that our as-received Lithium iodide was in its trihydrate form ($LiI.3H_2O$). The DTA showed a melting point of 105°C for lithium iodide trihydrate. The DTA curve for $LiI.3H_2O$ showed two/three minor peaks which are not well understood.

The DTA of mixed crystals containing 50 and 92 m/o $LiI.3H_2O$ showed only one peak each at 101°C and 85°C respectively has been modified and which probably corresponds with their respective melting points. A lowering of melting point is expected due to dissolution of foreign atoms or ions. Another interesting feature of the DTA of these compositions (50 and 92 m/o $LiI.3H_2O$) is that there are no more thermal events(peaks) corresponding to the dehydration of the salts (70 and 106°C, for example, in $LiClO_4.3H_2O$). This would suggest that either the water of hydration is no more there because the mixed crystals were heated at 90°C for several hours to allow the solid state reaction to take place or the mixed crystals have greater affinity towards the water of hydration. This point needs further investigation to

arrive at a definite conclusion.

The sample containing 8 m/o $LiI.3H_2O$ has two thermal events at 67.5°C and 112.5°C. The one at 67.5°C can be safely assigned to the dehydration of $LiClO_4.3H_2O$. In the pure $LiClO_4.3H_2O$, this event occurs at a slightly higher temperature (70°C). The other peak (≈ 112.5°C) corresponds to the melting of the mixed crystal which has been lowered from 145°C for the pure $LiClO_4.3H_2O$, as expected due to dissolution of impurity ions.

In summary, the XRD and DTA results are in conformity with each other in that both suggest the absence of a new phase and the complete solubility of at least 8 m/o $LiI.3H_2O$ in $LiClO_4.3H_2O$ at room temperature.

3.3 Heat Treatment and Thermal History :

The system under investigation ($LiClO_4.3H_2O$-$LiI.3H_2O$) was found to be very sensitive to the heat treatment in the sense that annealing time had a marked effect on the conductivity of the samples. In general the freshly pelletized samples show a higher conductivity than the annealed pellets at the same temperature. This could be due to two factors: (i) The presence of water is known to increase the conductivity. Thus a freshly prepared but unannealed pellet initially shows a higher conductivity which keeps on decreasing as the samples partially loose the water of hydration. (ii) The presence of grain boundaries is also known to increase the conductivity. Prolonged annealing tends to reduce the grain boundaries and hence conductivity.

Thus in order to obtain reproducible and reliable conductivity values, it was important to anneal the samples just below the melting point of system for several hours. Annealing of the samples sandwiched between the two electrodes is also advantageous from another point of view. It renders the electrode/solid contact in a much better shape.

In case of $LiClO_4$-LiI. $3H_2O$ system, the conductivity measurement was done both in air and in the glove box containing purified nitrogen atmosphere. In both the cases the effect of heat treatment on conductivity as mentioned above was noticed. However the effect of annealing time had more pronounced effect on sample resistances in case of air than that of the controlled atmosphere. This could be due to presence of more moisture in these samples. Both $LiClO_4$ and LiI are very hygroscopic materials. Since it was not possible to anneal the samples above 100°C - 110°C due to softening of pellets, it could not be expected to free the samples from moisture. In the case of glove box measurements this problem was minimized to a large extent because the nitrogen atmosphere was really free of moisture and accordingly the measurements were more reproducible. The samples were usually annealed overnight for 12 hrs.

The thermal history of the samples had also marked effects on the conductivity values. Barring few samples measured in the glove box, the conductivity measurements usually were less reproducible with respect to cooling and heating cycles. The conductivity values measured in the cooling cycle were generally higher than those in heating cycle. The rate of heating or cooling was also found to affect the conductivities of the samples. Higher cooling rate

generally yielded higher values of the conductivity. Those observations can be explained as follows; During the cooling cycle the lattice defects must continually disappear. As the crystal is cooled the defects are rendered less mobile and the time required to establish equilibrium becomes long. A point comes at which the concentration of defects becomes effectively independent of temperature (Jost, 1933), the time to establish equilibrium having become longer than the time required to measure the conductivity. To avoid this the cooling and heating rates were kept sufficiently low, nearly 10 degree/hr, so as to ensure that the samples are in thermodynamic equilibrium while recording the impedance.

An important advantage of switching from air to glove box measurements was considerable improvement in the reproducibility of conductivity measurements during cooling and heating cycles.

3.4 Complex Impedance Analysis :

In an electrical conductivity measurement on an ionic conductor it is vital to separate the bulk properties from the electrode effects complex impedance and complex admittance analysis, or as it is often called impedance spectroscopy is very useful for this purpose. In order to determine the electrical conductivity the bulk resistance of the sample has to be taken together with the dimensions of the sample. A small signal a.c. measurement on such a electrical conductivity cell can be represented by a network of resistances and capacitances, the so called equivalent RC circuit.

The simple models for cells with blocking and non- blocking electrodes discussed in the preceeding Chapter have been shown to agree fairly well with the experimental results for single crystal samples, e.g., for AgCl cells (R.P. Buck, D.E. Mathis , 1977), but also for some polycrystalline samples. In many cases, however, we get deviations from the impedance plots predicted by the model. In the $LiClO_4.3H_2O$ - $LiI.3H_2O$ system the majority of impedance plots are of this type, as shown in Figure 3.6. In this case we obtain a straight line at low frequencies characteristic of a double layer capacitance, but the line has an angle towards the real axis that is less than 90°. This type of impedance plot is attributed to the roughness of the electrode-electrolyte interface, the angle towards the real axis decreases with perfectly flat surfaces. This type of frequency response can be represented by a constant phase element (CPE), (J.C. Wang and J.B. Bates 1986) which has an impedance $Z = A\ (j2\pi f)^{-n}$ where n has a value between 0 and 1 and, A is a constant. Recently a model (S.H. Liu, T. Kaplan and L.J. Gray, 1986) using fractal theory to describe the electrode electrolyte interface has shown that the equivalent circuit for a Cantor-bar model of the surface has the CPE behaviour. Another model describing surface roughness as pores on the electrode also shows the CPE behaviour. Another effect is adsorption on electrode surfaces (Archer and Armstrong, 1980).

For a polycrystalline sample we may get a contribution to the impedance due to the presence of grain boundaries. The grain boundaries may act as a hindrance to the ion transport, but they might also provide a high conductivity path since the defect density may be larger in the interface region. In the first case

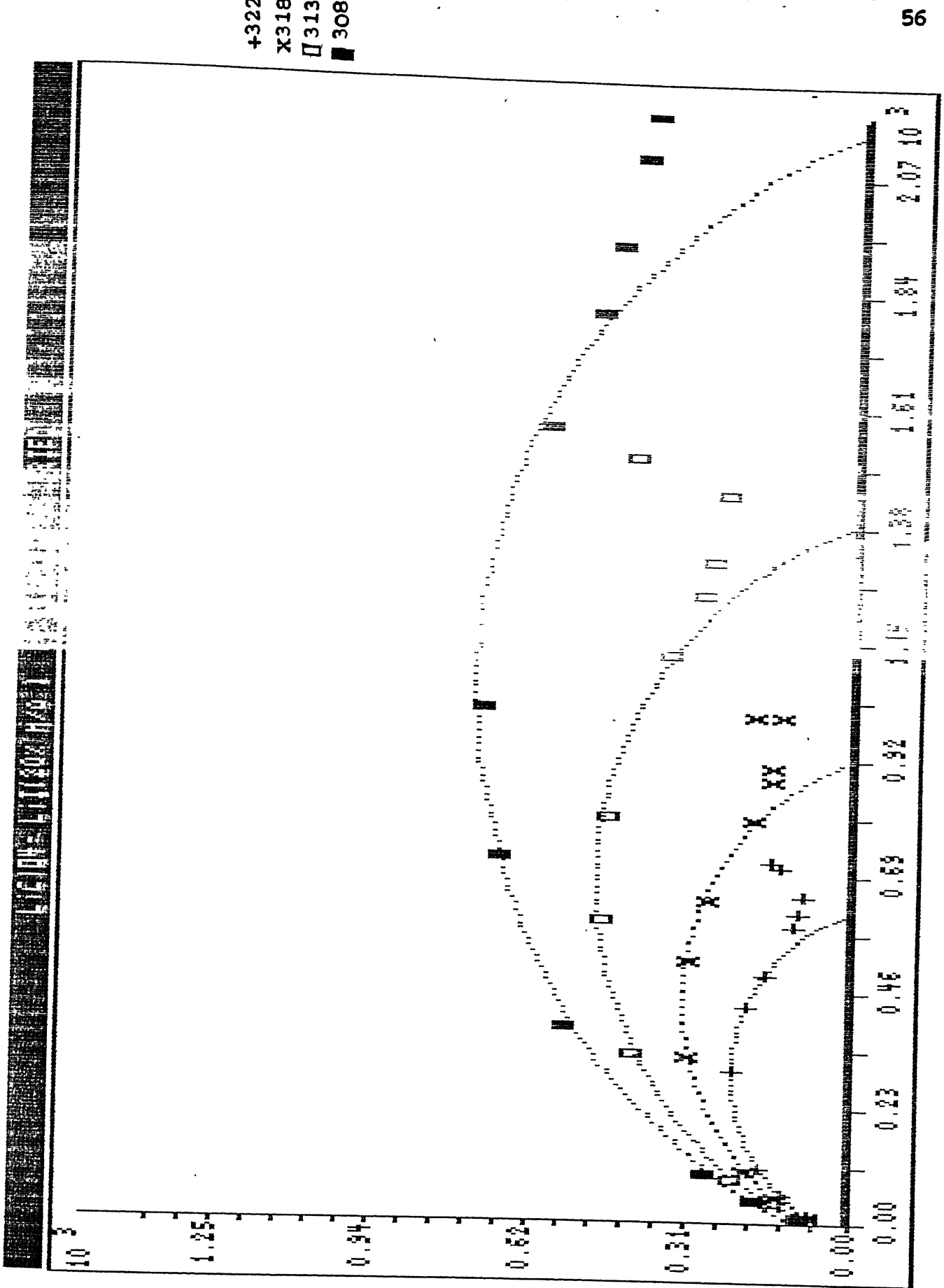

Fig. 3.6 Complex impedance plot

one can, in some cases, detect a second semicircle in the impedance plot representing grain boundaries. However this effect has not been found in the case of $LiClO_4$- LiI system in our experiment. The bulk resistance in such cases is obtained from the intersection of the high frequency impedance semicircle with the real axis. If we have an increased conductivity along the grain boundaries it will give an apparent bulk resistance that is lower than the real bulk effect.

In $LiClO_4.3H_2O$ - $LiI.3H_2O$ system, a large majority of the complex impedance plots were of the type shown in Figure 2.6 in which the diameter of the semicircle yields the d.c. resistance of the sample. However, in some cases, particularly at higher temperatures when samples become more conducting, the complex impedance plots are more or less straight line segments making an angle of less than 90° with the real axis (Figure 3.7). Such plots would suggest that the samples at higher temperatures behave simply as a constant phase element(CPE).

3.5 Electrical Conductivity of Pure Crystals :

The main objective of the present investigations was to study the ionic transport properties of the $LiClO_4$.LiI system and examine the effect of wrong size (homovalent) dopants on the ionic conductivity of the host salt, and also to identify any new intermediate highly conducting solid electrolyte that may be present in this system. Obviously the investigation was centred around the electrical conductivity measurements, the XRD and DTA measure-

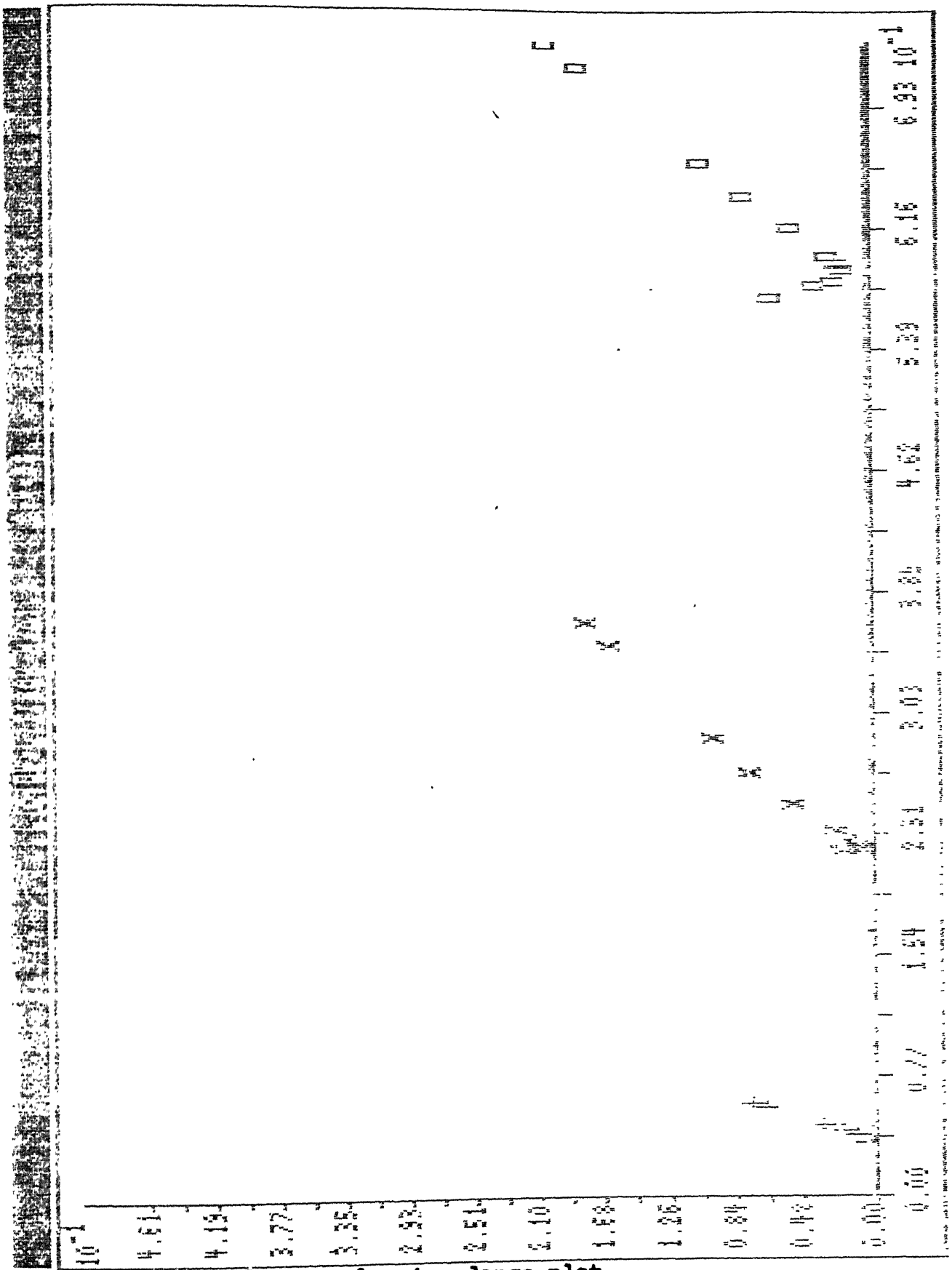

Fig. 3.7 Complex impedance plot

ments were carried out essentially to identify the various phases present in the mixed double salt $LiClO_4$.LiI. The results of electrical conductivity measurements on pure starting components are presented first followed by those on mixed systems, $LiClO_4 . {}^3H_2O$ + LiI. ^3H_2O.

3.5.1 Pure $LiClO_4 . {}^3H_2O$:

$LiClO_4$ has also been extensively used (Gabano, 1983) as solute in organic solvents to produce liquid electrolytes (Li^+ ion) for batteries. It was therefore quite surprising not to find much in the literature about the solid state properties of $LiClO_4$. However it is clear from the liquid electrolyte work that $LiClO_4$ is essentially an ionic solid in which the electronic conduction is negligibly small. Although there is no report of transference number measurements in the $LiClO_4$, the large difference between the ionic radii of Li^+ (0.68A°) and ClO_4^- (2.00A°) (L.Pauling, 1945) would suggest that the larger ClO_4^- ions would be far less mobile than the smaller Li^+ ions. Thus it is expected that almost all of the current is carried by Li^+ ions. This will be true for LiI as well. The lithium perchlorate used in the present investigation was in its trihydrate form, i.e., $LiClO_4 . {}^3H_2O$, as discussed in Section 3.1. $LiClO_4 . {}^3H_2O$ has hexagonal structure, the unit cell is shown in Fig. 3.8.

The electrical conductivity of $LiClO_4$ as a function of inverse absolute temperature is shown in Figure 3.9. As expected, the logσ vs $10^3/T$ plot consists of three distinct linear segments. The segment at the lower temperatures may be associated with the grain boundary conduction and that in the intermediate temperature

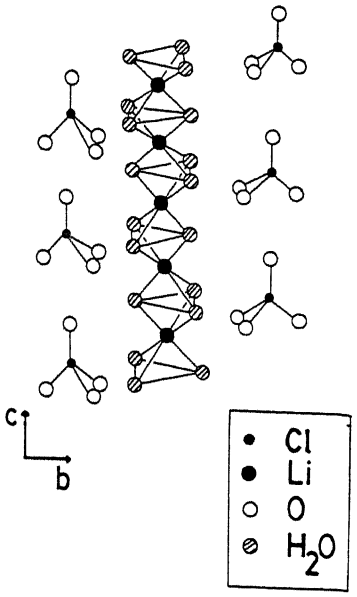

(a) The crystal structure of $LiClO_4 .3H_2O$

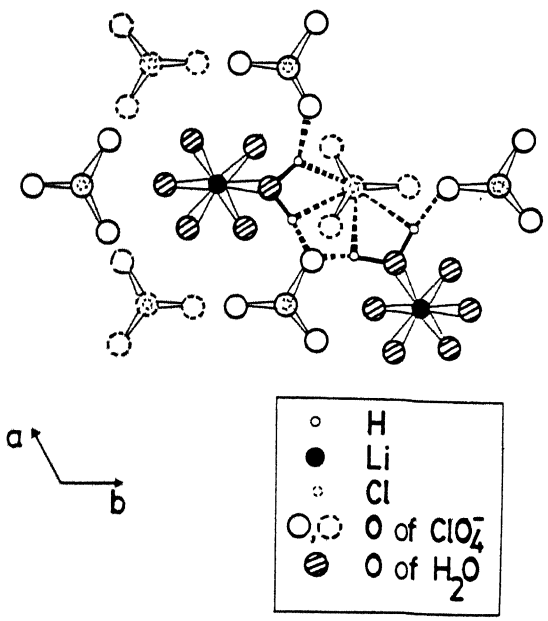

(b) The ab-plane and H-bonding in $LiClO_4 .3H_2O$

Fig. 3.8 Structure of $LiClO_4 .3H_2O$

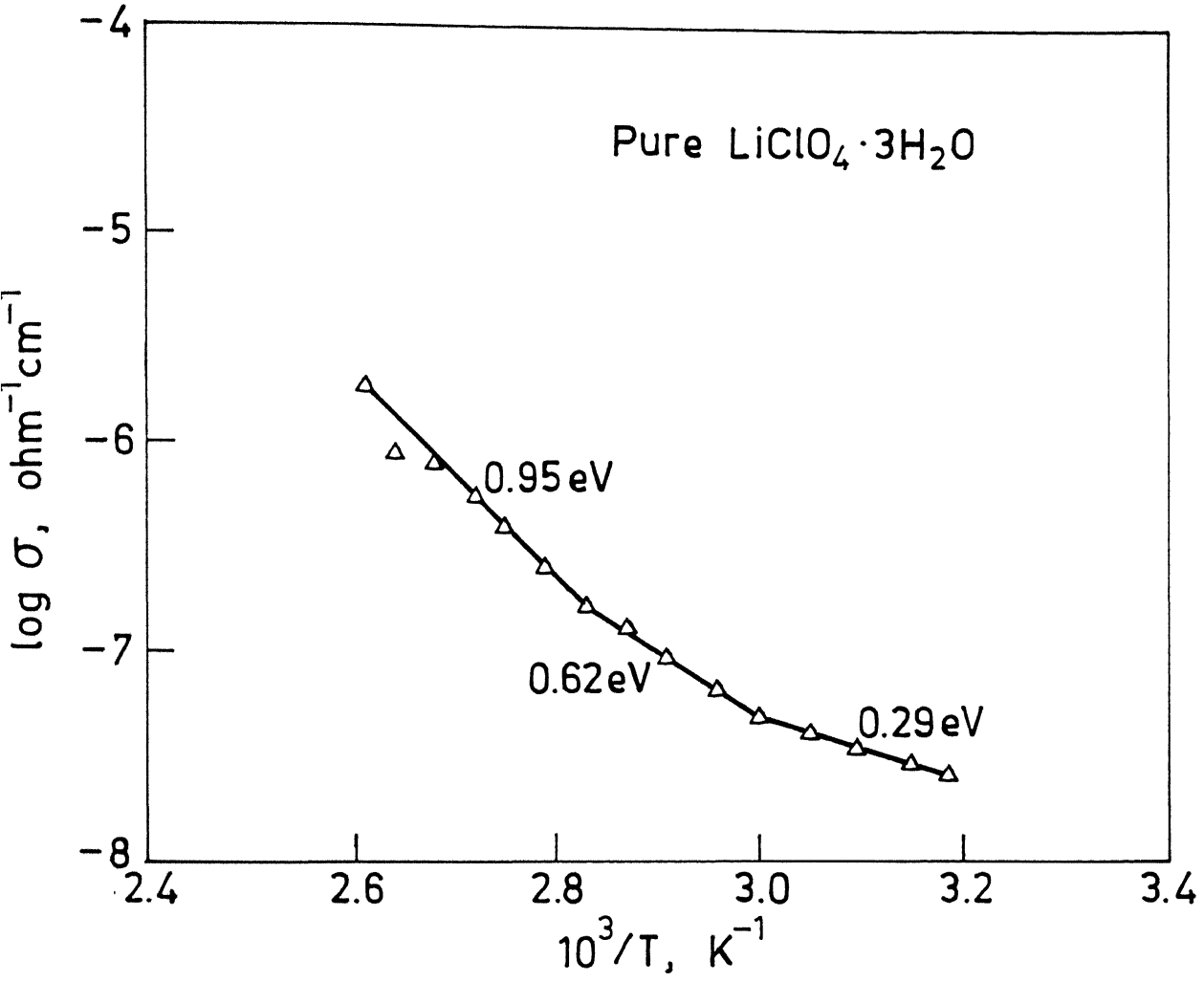

Fig. 3.9. Electrical conductivity vs inverse of temperature of pure $LiClO_4$ (air).

range, with the extrinsic or impurity controlled regions, and the associated slope can be used to calculate the migration energy of the most mobile species, Li^+ ions. The $\sigma(T)$ behaviour in the three regions can be described by the following equations :

$$\sigma = 1.353 \times 10^{-3} \exp\left(\frac{-0.29 \text{ eV}}{kT}\right) ; \quad 41° - 60°C \quad (3.1)$$

$$\sigma = 111.23 \exp\left(\frac{-0.62 \text{ eV}}{kT}\right) ; \quad 60° - 80\ °C \quad (3.2)$$

$$\sigma = 6.31 \times 10^{6} \exp\left(\frac{-0.95 \text{ eV}}{kT}\right) ; \quad 80.1° - 110°C \quad (3.3)$$

The Eqn. (3.2) yields an activation energy for migration (h_m) of Li^+ ions of 0.62 eV. The slope of linear segment at higher temperature yields :

$$h_m = 0.62 \text{ eV}$$

$$\frac{h_F}{2} + h_m = 0.95 \text{ eV}$$

or $$h_F = 2(0.95 - h_m) = 0.66 \text{ eV}$$

where h_F is the enthalpy of formation of Frenkel defects. It is apparent from Figure 3.9 that $LiClO_4 . 3H_2O$ does not possess any phase transition which is consistent with the DTA results (Section 3.2). The two thermal events observed in DTA of $LiClO_4 . 3H_2O$ (Table 3.4) were associated with dehydration of the material, and as such they do get reflected in the conductivity plot of Figure 3.9. A recent calorimetric experiment (White and Nightingale

1985) also finds no evidence for any phase transition.

3.5.2 Pure $LiI.3H_2O$:

All lithium halides LiX (X = F, Cl, Br, I), exhibit Schottky disorder even though the ionic radii of the halides and lithium ions are far from being comparable. It is usually agreed, however, that Li^+ vacancies are more mobile than X^- vacancies. The conductivity of the Lix is in the following order :

$\sigma_{LiF} < \sigma_{LiCl} < \sigma_{LiBr} < \sigma_{LiI}$. The room temperature conductivities of polycrystalline materials are in the order :

LiF	LiCl	LiBr	LiI	
10^{-12}	10^{-10}	10^{-9}	10^{-7}	$(Ohm\text{-}Cm)^{-1}$

These halides are highly hygroscopic and are stable in different hydrated forms. The ionic conductivities of these hydrates are in general higher than those of anhydrous ones. The LiI used in this investigation was identified by the XRD pattern to be in the form of $LiI.3H_2O$ having hexagonal structure.

LiI has been widely investigated and a lot of literature is available on the ionic conductivity of LiI in crystalline form. However we have reinvestigated the electrical conductivity of LiI for two reasons. First to have a comprehensive study of the $LiClO_4.3H_2O$ - $LiI.3H_2O$ system and secondly the data on $LiI.3H_2O$ are not so numerous. Two types of $LiI.3H_2O$ samples have been studied, one that was dried under vacuum before pelletization and the other as received from the manufacturer. The measurements were carried out

in the glove box. The results are shown in Figure 3.10. It is evident that there is very little difference between the conductivities of the samples. Also the activation energies are in good agreement with the experimental error. This would suggest once again that drying does not make much of a difference and that the dried salt is still $LiI.3H_2O$. A similar conclusion was arrived at based on XRD and DTA results.

The log σ vs $1/T$ results shown in Figure 3.10 consists of two linear segments. The low temperature linear segment can be associated with the so called extrinsic region and the high temperature segment with the intrinsic region. The σ (T) behaviour in the two regions can be expressed by the following equations for the dried samples:

$$\sigma = 2.3 \times 10^{6} \exp\left(-\frac{0.77\ eV}{kT}\right), \quad 38\text{-}97^{\circ}C \qquad (3.4)$$

$$\sigma = 4.0 \times 10^{20} \exp\left(-\frac{1.82\ eV}{kT}\right), \quad 97\text{-}132^{\circ}C. \qquad (3.5)$$

Thus the activation energy for migration of Li^{+} vacancies is found to be h_m = 0.77 eV and the energy of formation of schottky defects (h_s) is calculated to be :

$$\frac{h_s + h_m}{2} = 1.82\ eV$$

$$\text{or} \quad h_s = 2\,(1.82 - h_m) = 2.05\ eV$$

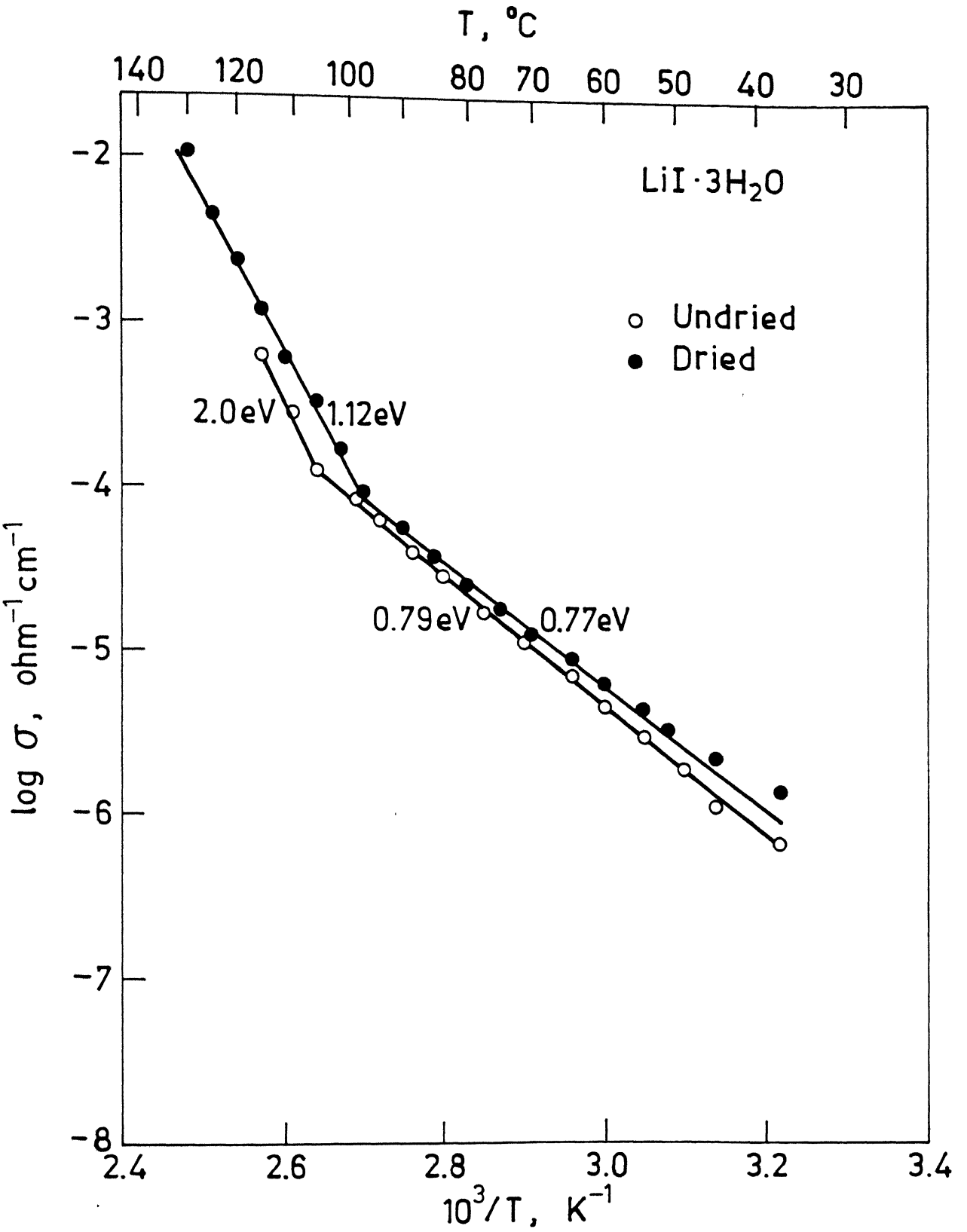

Fig. 3.10. Electrical conductivity vs inverse of temperature of pure LiI (glove box).

Our results agree well with those reported in literature. Bishop et.al (1966) have reported a conductivity of 3×10^{-6} $Ohm^{-1}Cm^{-1}$ at 50°C which is very close to our (2.8×10^{-6} $Ohm^{-1}Cm^{-1}$) value.

3.6 Conductivity of Mixed Crystals :

The aliovalent dopants, ie.e, foreign ions having a valency different from the corresponding host ion, e.g., Cd^{2+} in NaCl or Na^{+} in MgO, have long been used to enhance the ionic conductivity and control the type of defects which provide a very convenient way of determining the various transport parameters. However all these studies ignore the effect of the wrong size of the dopants which is invariably there alongwith the dopant. In fact the effect was considered negligible. However, recent experiments on various systems including KBr- KI, AgBr-AgI, LiBr-LiI, etc. have shown that the effect of the wrong size in general is not negligible and in some cases significant enough to warrant a reanalysis of the entire old results. Since $LiClO_4 . 3H_2O$- $LiI . 3H_2O$ system involves the substitution of I^- ions in place of ClO_4^- ions which are in the same valency state, any change in conductivity has to be accounted for in terms of the wrong size of the dopant alone. Thus an investigation of this system will offer another opportunity to substantiate the effect of wrong size on the ionic conductivity. Shahi and Wagner (1982) have proposed that the effect of homovalent doping can be explained on the basis of lattice loosening created by the introduction of homovalent (wrong size) impurities which tends to lower the melting points of the salts and hence decreases the enthalpy of formation of a defect pair and thereby increases the conductivity. The

results of $LiClO_4 . 3H_2O$ + $LiI . 3H_2O$ system can also be useful to test the above model.

3.7 Conductivity Measurements in Air :

The conductivity measurement was initially started in air using two kinds of samples, one using the as-received starting materials, $LiClO_4$ and LiI and melting the mixtures and the other using the predried starting materials and then heating the mixture at 100°C for 9 hrs (solid state reaction). These two samples are referred to as undried and dried respectively

It must be pointed out that numerous problems were encountered during the investigation primarily because of the very hygroscopic and to some extent reactive nature of the starting materials. For example, it was noticed during the conductivity, experiments that the samples swelled significantly and even reacted with ss electrodes. The heavy swelling could have been due to the melting of at least one of the phases viz. $LiI.3H_2O$, when working between 100° to 120°C.

Rather surprising conductivity results were obtained when measurements were carried out in air. These results are shown in Figure 3.11 for 10 m/o $LiI . 3H_2O$ and in Figure 3.12 for 15 m/o $LiI.3H_2O$ (both undried samples) and in Figure 3.13 for 8 m/o $LiI . 3H_2O$ (dried). In all cases a peculiar result was that the conductivity was found to increase with decreasing temperature in certain temperature regions. This is not well

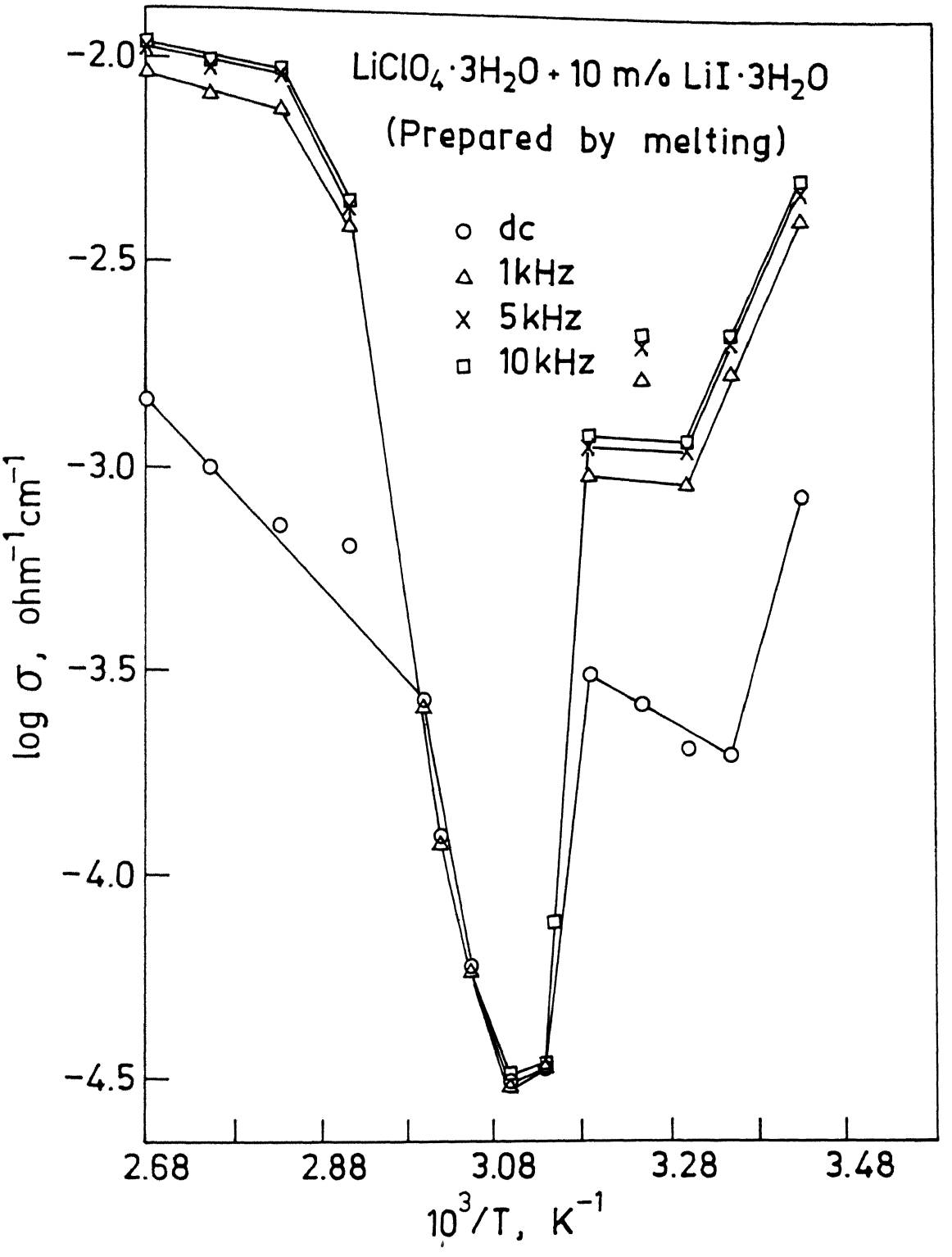

Fig. 3.11. Electrical conductivity vs inverse of temperature (air).

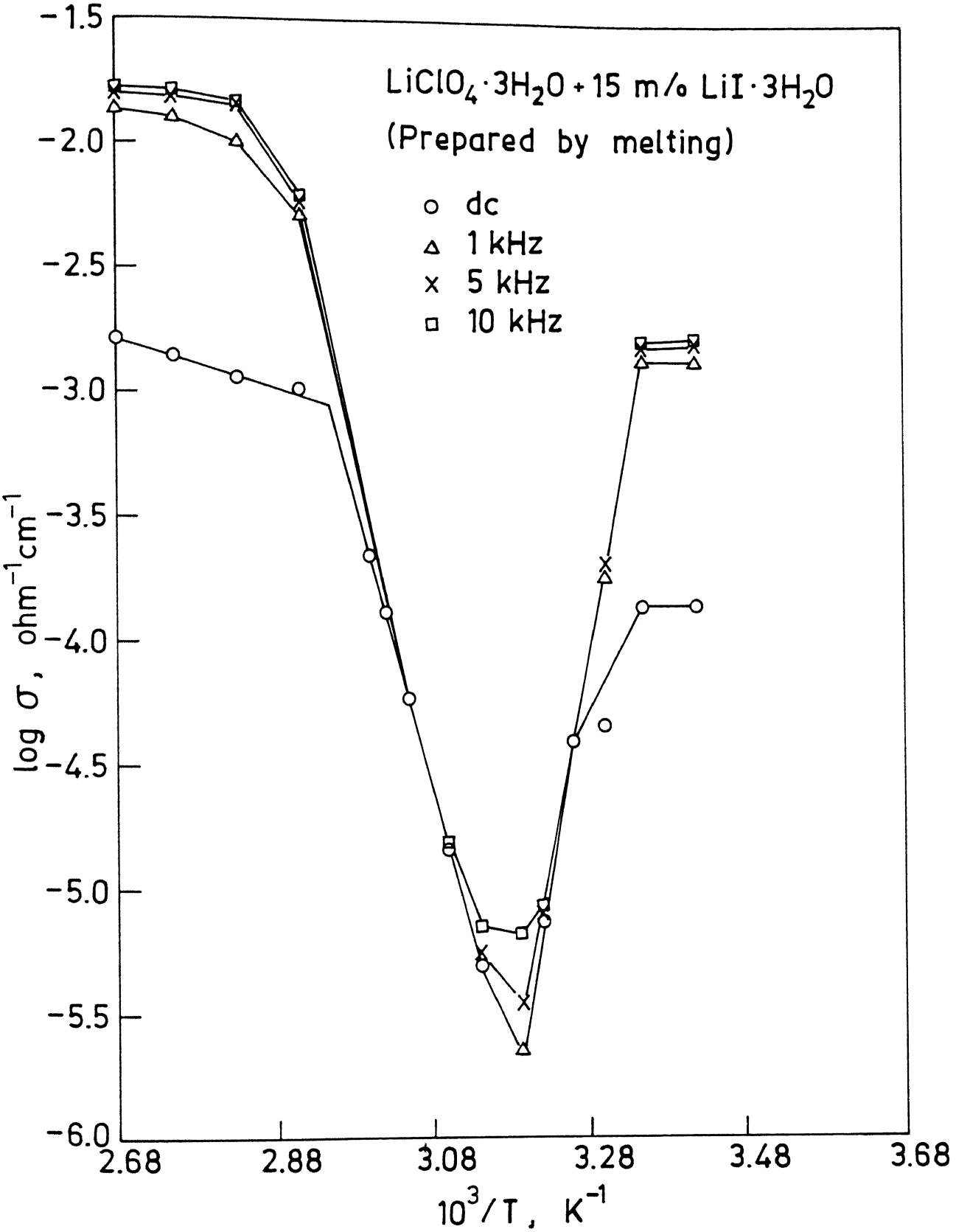

Fig. 3.12. Electrical conductivity vs inverse of temperature (air).

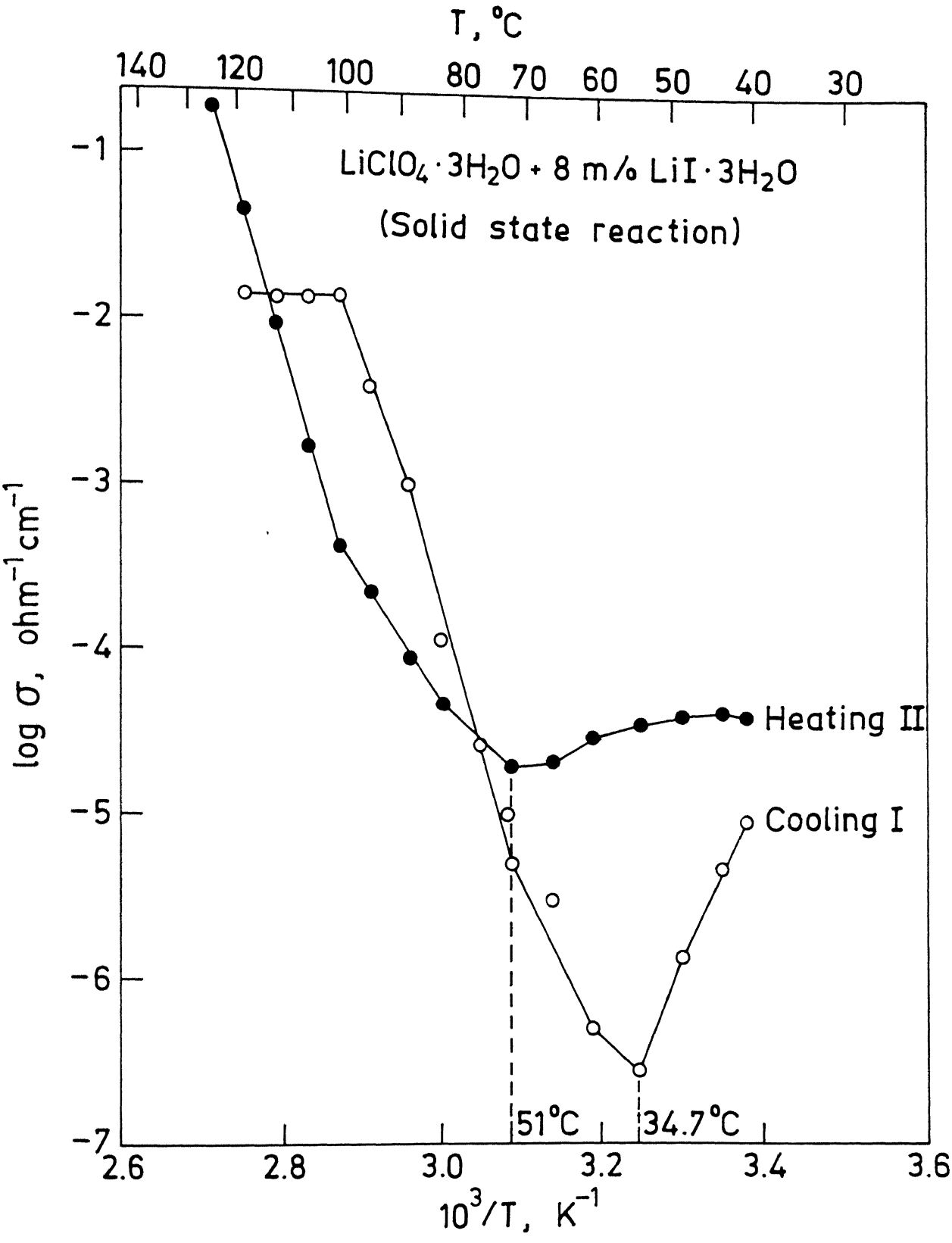

Fig. 3.13. Electrical conductivity vs inverse of temperature (dried sample, air).

understood at present, but it is suspected that it may be due to some decomposition of the materials. The temperature ranges in which this peculiar behaviour was observed are mentioned below:

Sl. No.	Sample	Temperature range, °C	Swing in conductivity $(\Omega\text{hm-Cm})^{-1}$
1	10 m/o $LiI.3H_2O$(undried)	49.6 to 18.5	2.15×10^{-6} to 1.34×10^{-4}
2	15 m/o $LiI.3H_2O$(dried)	40.5 to 19.4	2.98×10^{-5} to 8.8×10^{-4}
3	8 m/o $LiI.3H_2O$ (dried)	34.7 to 22.8 (cooling)	2.66×10^{-7} to 8.5×10^{-6}
		51.0 to 22.8 (heating)	2.00×10^{-5} to 3.9×10^{-5}

Further, the σ (T) plots shown in Figures 3.11 and 3.12 exhibit a sharp minimum which shifts to lower temperature as the concentration of $LiI.3H_2O$ in the undried samples increases. Also the temperature range in which the peculiar behaviour was observed tends to narrow with the increasing concentration of LiI. At first sight the valley in the σ (T) plots (Figures 3.11 and 3.12) appears to be associated with a major phase transition. However DTA did not indicate the presence of any such transition. This aspect would need further investigation.

Because of the limited time the experiment was switched over to the controlled atmosphere glove-box and all subsequent studies were carried eut in highly purified dry nitrogen gas.

3.8 Conductivity Measurements in the Controlled Nitrogen Atmosphere Glove Box :

3.8.1 Conductivity vs Composition :

As mentioned before, two types of samples, calledundried and dried, were used. Figures 3.14 and 3.15 show the conductivity as a function of composition (mole % of $LiI.3H_2O$ added in $LiClO_4.3H_2O$) at several different temperatures (35°, 50°, 75° and 100°C). In Figures 3.14 and 3.15, it is observed that there is a sharp rise in the conductivity by the addition of $LiI.3H_2O$ in $LiClO_4.3H_2O$. For the undried samples $\sigma(T)$ curves exhibit a maximum around 50 m/o $LiI.3H_2O$ and thereafter the conductivity decreases with increasing concentration of $LiI.3H_2O$. The enhancement in conductivity is by a factor of 100 to 1000, the maximum enhancement by a factor of 100 is observed at 100°C. The sample, $LiClO_4.3H_2O$ + 50 m/o $LiI.3H_2O$ was found to exhibit a maximum conductivity of 3×10^{-3} $Ohm^{-1}Cm^{-1}$ at 100°C and 10^{-4} $Ohm^{-1}Cm^{-1}$ at 50°C, which is a significant improvement over the conductivity of pure $LiClO_4.3H_2O$ (10^{-6} $Ohm^{-1}Cm^{-1}$). The conductivity composition plots (Figure 3.15) for dried samples also show a sharp rise in the conductivity for smaller concentrations of the dopant. However there is a marked difference between these results and those for undried samples (Figure 3.14) in that the conductivity goes through a minimum around 50 m/o LiI in case of dried samples which is absent in case of undried samples. Also the maximum enhancement in the conductivity is less for dried samples than that of undried sample. However it should be pointed out that since the reproducibility of results was poor for undried samples and also other problems like swelling of pellets were more pronounced for these samples they

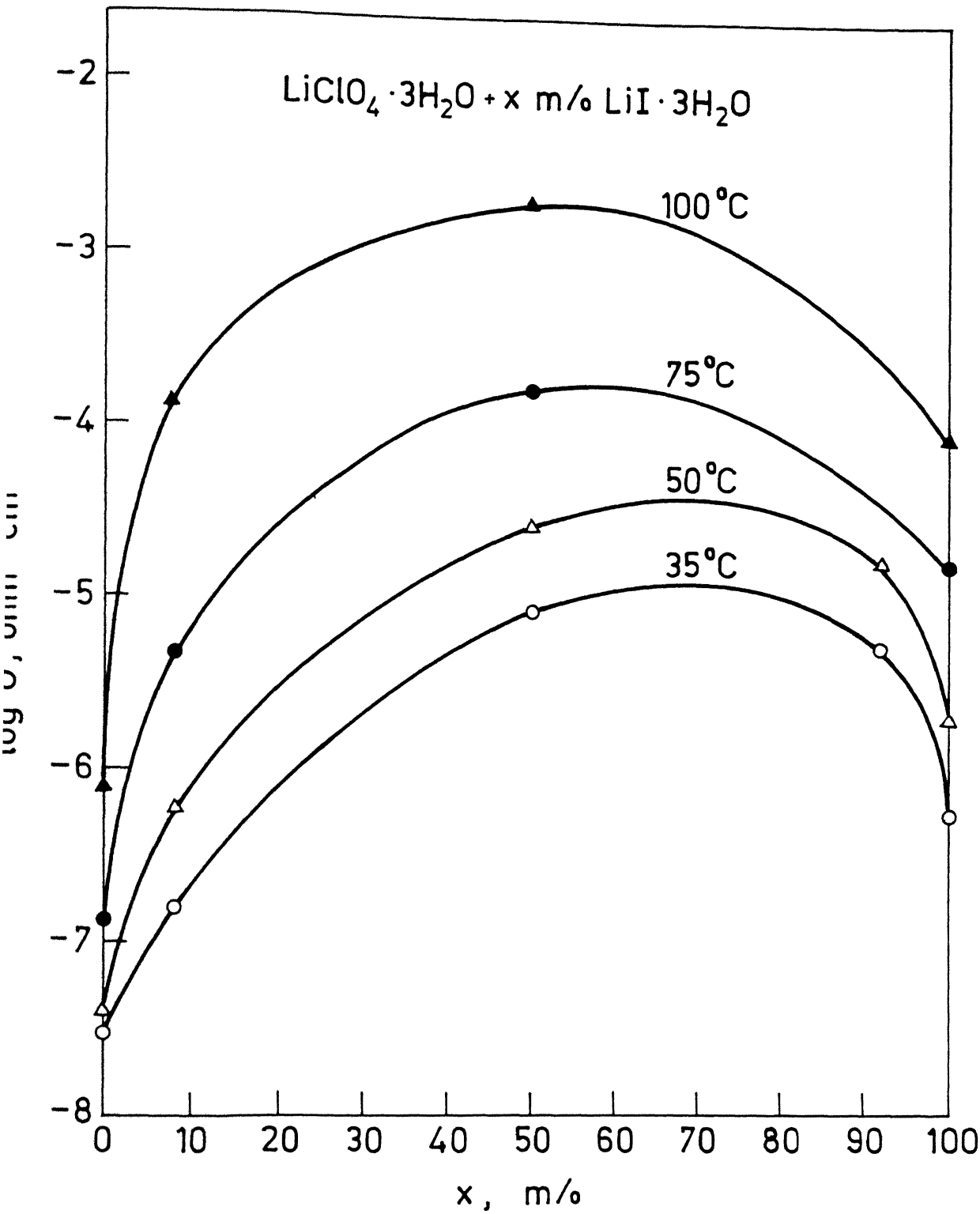

Fig. 3.14. Conductivity as a function of concentration of $LiI \cdot 3H_2O$ in $LiClO_4 \cdot 3H_2O$ (undried).

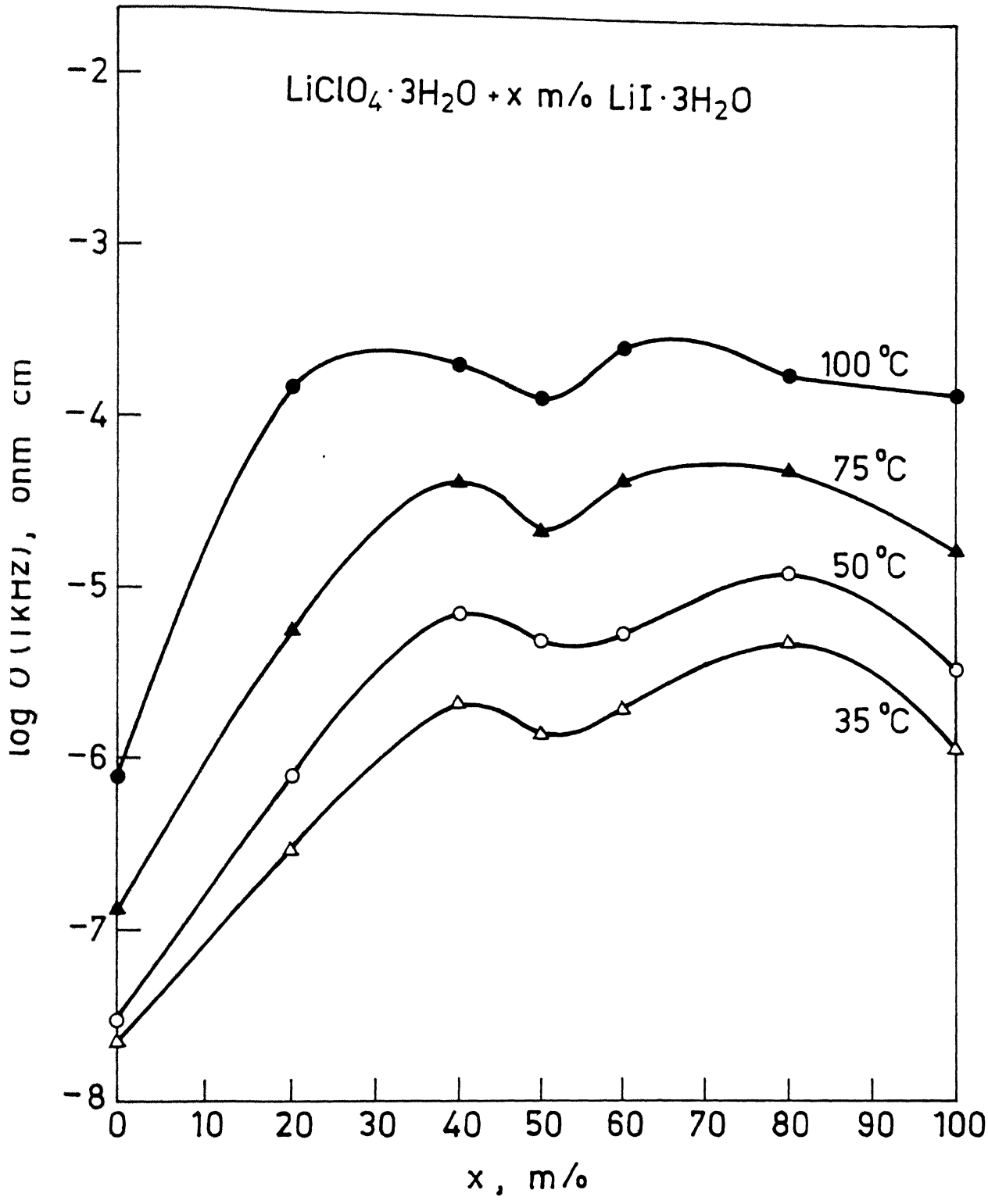

Fig. 3.15. AC(1kHz) conductivity as a function of concentration of $LiI \cdot 3H_2O$ in $LiClO_4 \cdot 3H_2O$ (dried).

were not studied so thoroughly. Thus a detailed comparision between the two results at this stage may not be desirable.

Figure 3.15 shows another σ vs composition plot for the dried samples. In this case the conductivity values are at 1 kHz, rather than dc values. These results are very much similar to those of Figure 3.16(dc values).

The results of Figures 3.14 and 3.16 together with the DTA and XRD results suggest that there is considerable enhancement in the conductivity due to substitution of wrong size I^- ions. These results are consistent with previous studies on various mixed crystals, which further substantiate the '' lattice loosening'' model of enhancement in the conductivity of homovalently doped crystals.

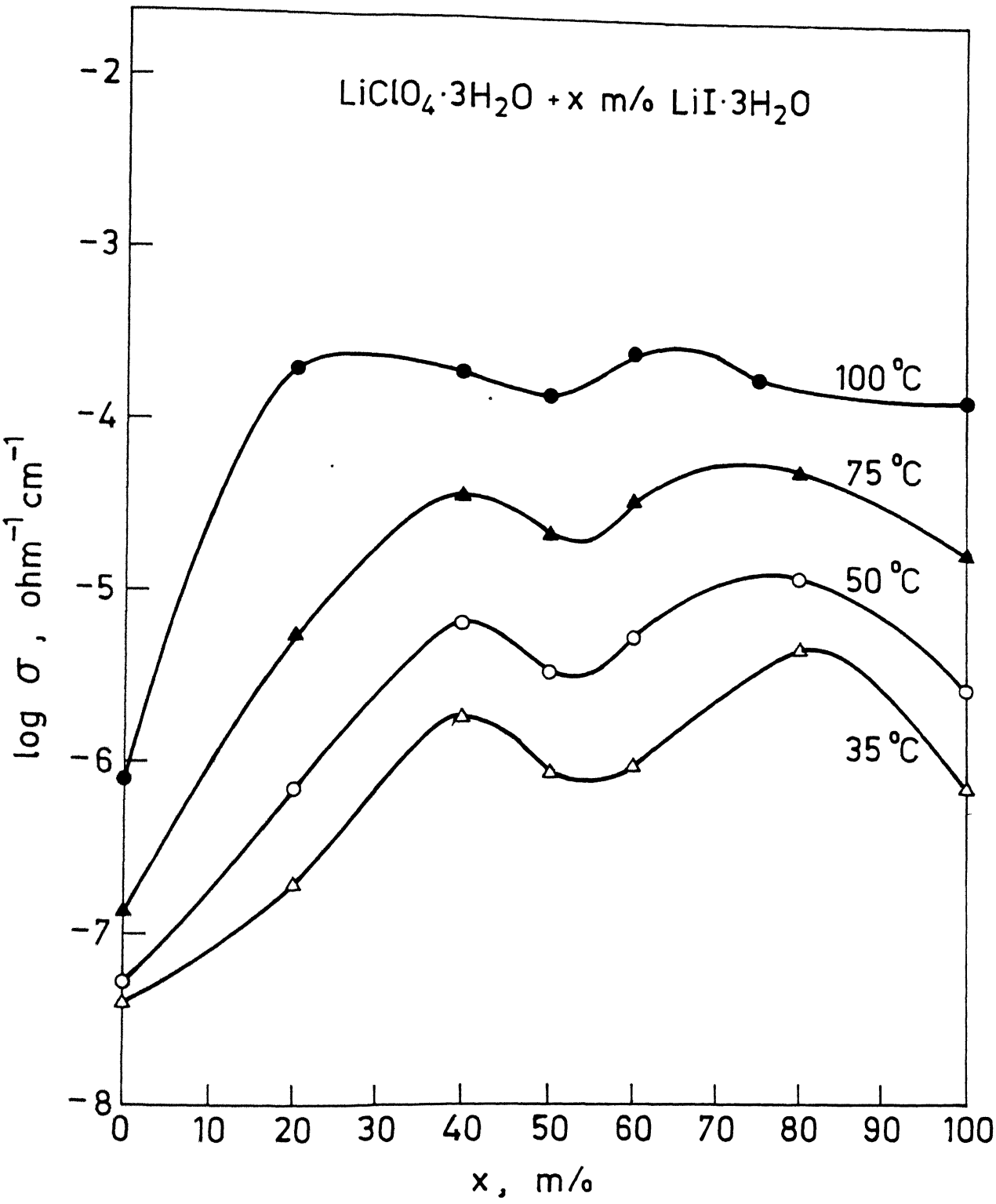

Fig. 3.16. Conductivity as a function of concentration of $LiI \cdot 3H_2O$ in $LiClO_4 \cdot 3H_2O$ (dried)

3.8.2 Electrical Conductivity versus Temperature :

Two types of samples were used for the conductivity measurements inside the glove box : one which was prepared using the as-received starting materials $LiClO_4$ and LiI. These are referred to as undried samples and three different compositions (8,50 and 92 m/o $LiI.3H_2O$) were studied. The second type of samples were prepared in the glove box using predried salts, as discussed earlier. These are termed "dried" samples, and 6 different compositions (8,20,40,50,60 and 80 m/o $LiI.3H_2O$) of these were investigated.

It should be pointed out that the samples $LiClO_4.3H_2O$ $LiI.3H_2O$ can either from single phase solid solutions, $Li(ClO_4)_{1-x}I_x (0 \leqslant x \leqslant 1)$, or else they can form a two-phase mixtures of $LiClO_4.3H_2O$ containing some dissolved I^- and $LiI.3H_2O$ containing some dissolved ClO_4^-. According to our XRD analysis which however is limited to room temperature only, $Li(ClO_4)_{1-x}I_x$ is a single phase (hexagonal) material for atleast upto 8 m/o $LiI.3H_2O$ ($x = 0.08$). The other compositions containing higher concentration of $LiI.3H_2O$ are two phase mixtures at least at room temperature, but it is quite possible that they become single phase at higher temperatures as the dissolution is strongly temperature dependent in general.

Figure 3.17 shows the conductivity vs $10^3/T$ plot for the undried samples. It is apparent that there is significant enhance

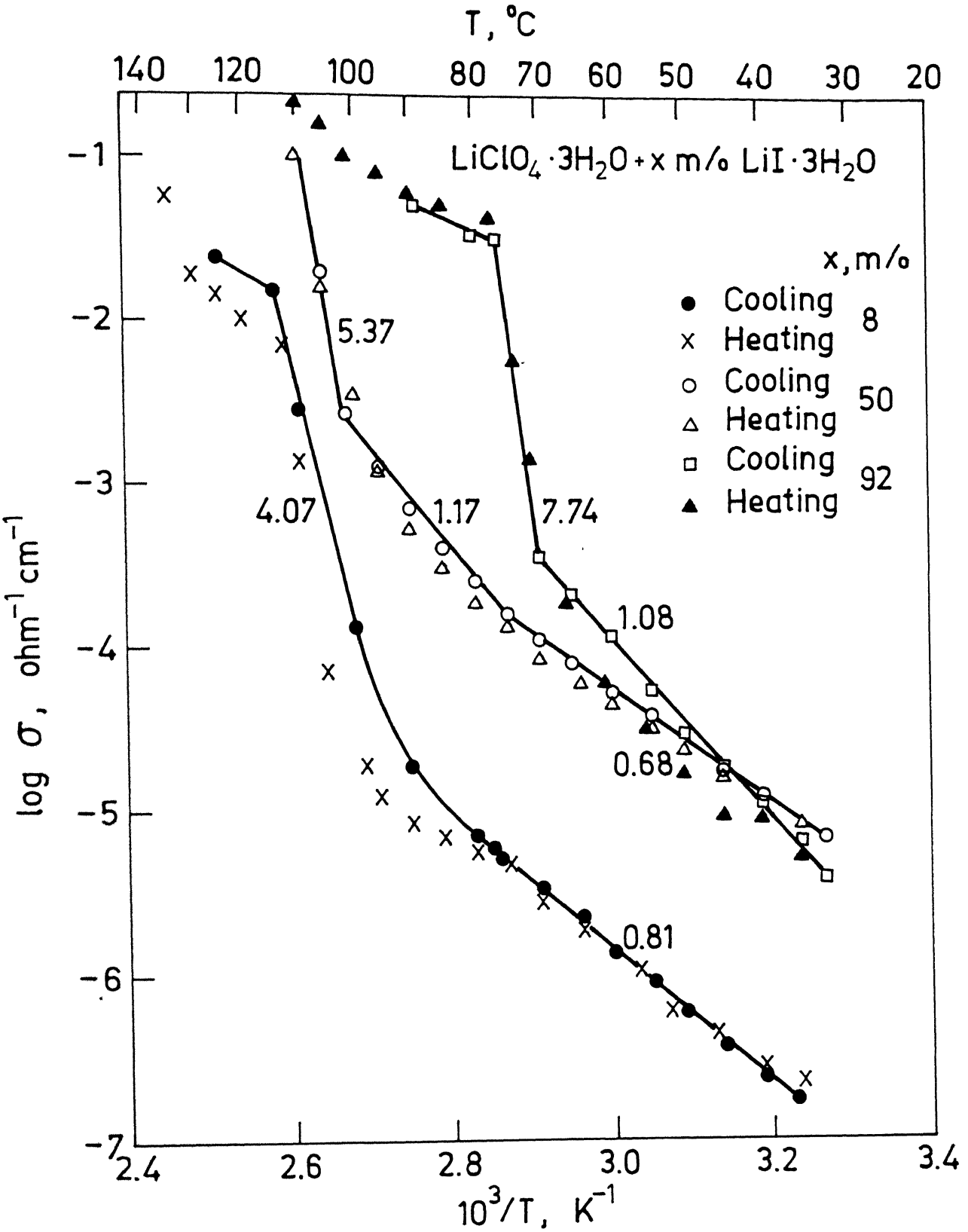

Fig. 3.17. Electrical conductivity vs inverse of temperature (undried).

ment in the conductivity due to addition of $LiI.3H_2O$ in $LiClO_4.3H_2O$. As pointed out earlier the sample containing 8 m/o $LiI.3H_2O$ is a single phase solid solution of $LiClO_4$ containing dissolved I^- ions. The log σ vs $1/T$ plot for this composition consists of two linear segments-extrinsic and intrinsic regions. The dissolved I^- ions do affect the activation energies and the extrinsic to intrinsic transition temperatures. However, there is no systematic dependence of activation energies (slopes of log σ vs $1/T$) on the dopant concentration.

A rather surprising feature of the mixed crystals is that they exhibit a region where conductivity changes extremely rapidly. Most probably these high temperature regions with apparent large activation energies are associated with pre-melting effect, i.e. the mixed crystals melt over a range of temperature and not sharply at a certain temperature as pure salts do.

The log σ vs $1/T$ plots for $LiClO_4.3H_2O$ + x m/o $LiI.3H_2O$ (x = 8,20,40,50,60 and 80 are shown in Figures 3.18 and 3.19. The main features of these results are essentially similar to those of undried samples shown in Figure 3.17; namely, there is appreciable increase in the conductivity due to the addition of $LiI.3H_2O$. However, as pointed out earlier, these results were far more reproducible than those for undried samples. These dried samples also display extrinsic and intrinsic regions of conduction in the log σ vs $1/T$ plot. The σ (T) behaviour of these samples can be described by the following equations.

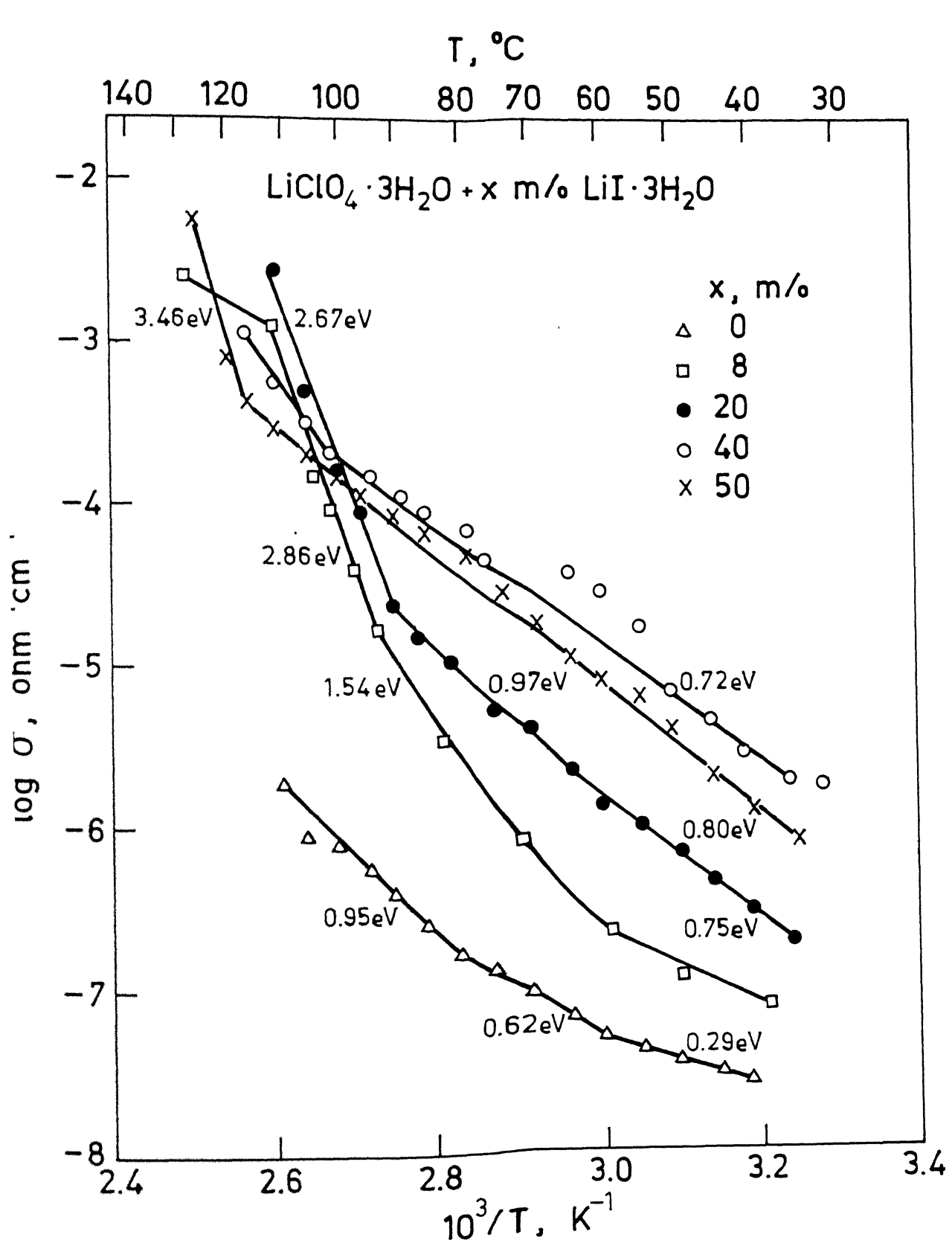

Fig. 3.18. Electrical conductivity vs inverse of temperature (dried).

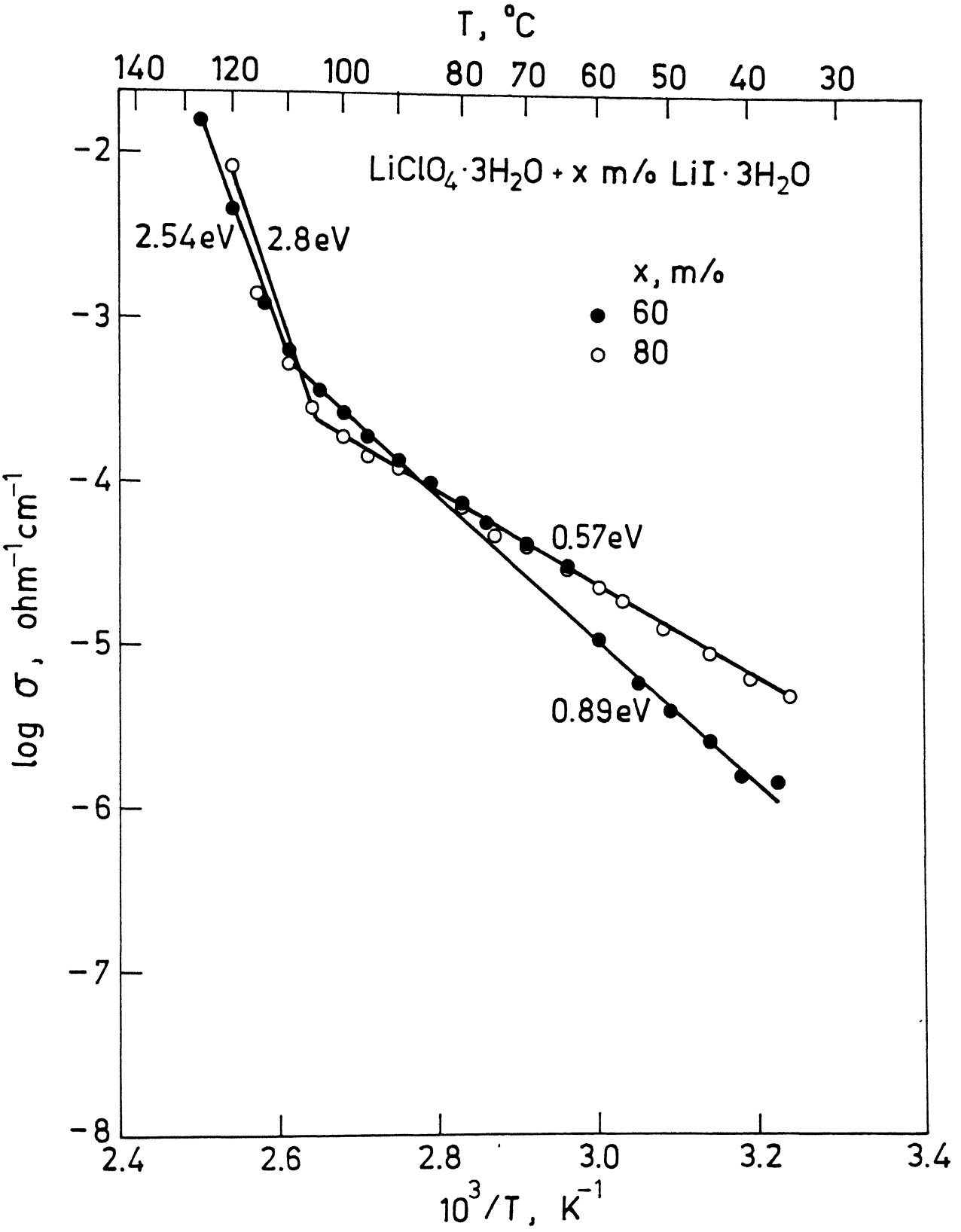

Fig. 3.19. Electrical conductivity vs inverse of temperature (dried).

$LiClO_4 . 3H_2O$ + x m/o $LiI.3H_2O$

x = 8, $\sigma = 1.38 \exp\left(\frac{-0.45}{kT}\right)$; 38° - 64°C (3.6)

$\sigma = 2.61 \times 10^{16} \exp\left(\frac{-1.54}{kT}\right)$; 64° - 93°C (3.7)

x = 20, $\sigma = 3.11 \times 10^{5} \exp\left(\frac{-0.75}{kT}\right)$; 35°- 64°C (3.8)

$\sigma = 7.13 \times 10^{8} \exp\left(\frac{-0.97}{kT}\right)$; 64° - 90°C (3.9)

x = 40, $\sigma = 1.0 \times 10^{6} \exp\left(\frac{-0.72}{kT}\right)$; 35° - 101°C (3.1

$\sigma = 7.24 \times 10^{4} \exp\left(\frac{-1.38}{kT}\right)$; 101°- 116°C (3.1

x = 50, $\sigma\ 9.38 \times 10^{6} \exp\left(\frac{-0.80}{kT}\right)$; 34° - 116°C (3.1

x = 60, $\sigma = 2.73 \times 10^{8} \exp\left(\frac{-0.89}{kT}\right)$; 37° - 110°C (3.1

x = 80, $\sigma = 9.26 \times 10^{3} \exp\left(\frac{-0.57}{kT}\right)$; 35° - 105°C (3.1

As in case of undried samples, the dried sample also exhibit high temperature regions in which the conductivity changes rapidly and these are attributed to premelting effects. The effect of dopants on the activation energy is once again not systematic.

3.8.3 Activation Energies for Formation and Migration of Defects :

The low temperature linear segment, usually called extrinsic region, in the the log σ vs $1/T$ plot can be used to obtain the migration energy of the mobile defect, Li^+ ion in case of $LiClO_4.3H_2O$ and Li^+ ion vacancy in case of LiI. $3H_2O$. Similarly, the high temperature linear region, usually called intrinsic region, in the log σ vs $1/T$ plot yields the sum of half the formation energy (h_F) and the migration energy (h_m). Thus from the slopes of the two regions the activation energies h_F and h_m can be calculated. These together with the extrinsic to intrinsic transition (knee) temperatures, conductivity at the knee temperatures, the preexponential factors σ_o in $\sigma = \sigma_o \exp(- Ea/kT)$, etc. for both undried and dried samples are summarized in Tables 3.5 (a 3.5 (b), 3.6 (a), 3.6 (b) and 3.6 (c).

Table 3.5 (a) Electrical Transport Parameters of Undried $LiClO_4.3H_2O$ + $LiI.3H_2O$ Samples

S. No.	Composition (mole % of $LiI.3H_2O$)	Activation Energy E_a (eV)	Pre-exponential Factor σ_o ($Ohm^{-1}Cm^{-1}$)	Temperature Range (°C)
1	8	0.81	2.47×10^{6}	36-95
2	50	0.68	1.08×10^{6}	33-75
		1.175	1.26×10^{13}	75-101
3	92	1.08	2.4×10^{12}	32-70

Table 3.5 (b) Electrical Conductivity, Activation Energy and Extrinsic to Intrinsic Transition (knee) Temperature of Undried Samples

S. No.	Mole % of LiI	Activation Energy E_a	Knee Temperature T_c (K)	Conductivity σ_{T_c} ($Ohm^{-1}Cm^{-1}$)
1	0	0.29	333	5.0×10^{-8}
		0.62	353	1.7×10^{-7}
2	8	0.81	357	9.4×10^{-6}
3	50	0.68	348	1.6×10^{-4}
4	92	1.08	343	3.5×10^{-4}
5	100	0.79	378	1.2×10^{-4}

Table 3.6 (a) Electrical conductivity, activation energy and extrinsic to intrinsic (knee temperature of ddried samples

S. No.	Mole % of LiI	E_a (ev)	knee temperature(°C)	Knee conductivity σ_{tc}(Ohm^{-1}Cm^{-}
1	0	0.29	60	5.0×10^{-8}
		0.62	80	1.7×10^{-7}
		0.95	110	1.9×10^{-6}
2	8	0.45	65	2.8×10^{-7}
		1.54	93	1.7×10^{-5}
3	20	0.75	65	2.1×10^{-6}
		0.97	90	2.4×10^{-5}
4	40	0.72	101	2.1×10^{-4}
5	50	0.80	117	4.2×10^{-4}
6	60	0.89	110	5.6×10^{-4}
7	80	0.57	106	2.4×10^{-4}

Table 3.6 (b) Electrical Transport Parameters of Dried $LiClO_4$. $3H_2O$ + LiI. $3H_2$ Samples

S. No.	Composition mole % LiI. $3H_2O$	Activation Energy (E_a (eV)	Pre-exponential Factor σ_o (Ohm^{-1} Cm^{-1})	Temperature Range °C)
1	8	0.45	1.38	38-65
		1.54	2.61×10^{16}	65-93
2	20	0.75	3.11×10^{5}	35-65
		0.97	7.13×10^{8}	65-90
3	40	0.72	1.06×10^{6}	35-101
4	50	0.80	9.38×10^{6}	35-117
5	60	0.89	2.73×10^{8}	37-110
6	80	0.57	9.26×10^{3}	35-106

Table 3.(c) Energies of Defect Formation and Migration

S. No.	Mole % of LiI	Extrinsic Activation Energy E_a(eV)	Intrinsic Activation Energy E_a(eV)	Energy of Migration h_m (eV)	Energy of defec formatio h_s(eV)
1	0	0.62	0.95	0.62	0.66
2	8	0.45	1.54	0.45	2.18
3	20	0.75	0.97	0.75	0.44
4	40	0.72	1.38	0.72	1.32
5	50	0.80	-	0.80	-
6	60	0.89	-	0.89	-
7	80	0.57	-	0.57	-
8	100	0.77	1.82	0.77	2.10

CONCLUSION

$LiClO_4$ dissolved in organic solvents has been widely used as a liquid electrolyte in batteries. However there is very little work on $LiClO_4$ as a solid electrolyte. The reason for this might be, as we discovered during the investigation, the handling problem associated with this material. However some of these difficulties were overcome by us by making use of the moisture-controlled nitrogen atmosphere glove box. It should be noted here that both $LiClO_4$ and LiI are extremely hygroscopic and the as-received materials were in their trihydrate form. Both $LiClO_4 . 3H_2O$ and $LiI.3H_2O$ crystalize in hexagonal structures.

The XRD and DTA results indicate that the solubility of LiI in $LiClO_4$ is quite limited, perhaps less than 20 mole % at room temperature. Both $LiClO_4.3H_2O$ and $LiI.3H_2O$ are moderate ionic conductors at room temperature. The addition of $LiI . 3H_2O$ in $LiClO_4.3H_2O$ increases the electrical conductivity significantly. The enhancement is dependent on the thermal history of the samples and the method of preparation. The samples prepared by using the as-received (undried) materials showed enhancements by as much as a factor of 10^3. However these results were not very reproducible. Subsequently the preparation and measurements of conductivity were carried out inside the controlled atmosphere glove box. These so called dried samples were well behaved and also yielded better reproducibility. However the enhancement in the conductivity was less in this case than the previously undried samples.

REFERENCES

1. Archer, W.I., and Armstrong, R.D., in, Electrochemistry Vol. 7, ed. H.R. Thirsk (The chemical Society, London,1980).

2. Bates, J.B., Wang, J.C. and Chu, Y.T., Solid State Ionics 18 and 19, 1045 (1986).

3. Bhatnagar, S., Gupta, S., Shahi, K., Solid State Ionic Devices, eds. B.V.R. Chowdari and S. Radhakrishna (World Scientific Publishing Co. Pt. Lt., Singapore, 1988); pp. 393-398.

4. Bishop, S.G., Ring, P.J. and Bray, P.J., (1966). J. Chem. Phys. Vol. 45, 1525.

5. Buck, R.P., Mathis, D.E. and Rhodes, R.K., J. Electroanal. Chem. 80, 245 (1977).

6. Chandra, S., Superionic Solids : Principles and Applications (North Holland, 1981) 17.

7. Farrington, G.C., 'Solid State Batteries', ed. C.A.C. Sequeria and A. Hooper, pp 19-26 (1985).

8. Gabano, J.P.,' Lithium Batteries', Academic Press London (1983).

9. Geller, S. (1977), 'Solid Electrolytes' ed. Geller, Springer Verlag, Berlin.

10. Johannesen, Solid State Ionics 28-30 (1988) 1310-1316, North -Holland, Amsterdam.

11. Keeffe, M.O., 'Phase Transition and Translational Freedom in Solid Electrolytes in Superionic Conductors', ed. G.C. Mahan and W.L. Roth (Plenum Press, New York, 1979) p. 101.

12. Lidiard, A.B. (1957), Handbuch der Physik, Vol. 20, p-246, editor, S. Floog, Springer Verlag.

13. Liu, S.H., Kaplan, T. and Gray, L.J., Solid State Ionics 18 and 19 (1986) 65.

14. Mellander, B.E and Lunden, A.,'Materials For Solid State Batteries'(Proceedings of the Regional Workshop, Singapore 2-6 June 1986), p. 161-168.

15. Rice, M.J. and Roth, W.L., J. Solid State Chem. Vol. 4, 294 (1972).

16. Sequeria, A., Bernal, I , Brown, I.D. and Faggiane, R., Acta Cryst. B 31, 1735 (1975).

17. Shahi, K. and Wagner, J.B., (1982), J. Phys. Chem. Solids, Vol. 43, No. 8, pp. 713-722.

18. Shahi, K.,and Wagner, Jr., J.B., J. Phys. Chem. Solids Vol. 44. No. 2, pp. 89-94, (1983).

19. Shahi, K., and Wagner, J.B., Solid State Ionics 12 (1984), 511-516.

20. Wang et. al., J. Chem. Phys. 63, 722 (1975).

21. White, M. A. and Nightingale, K., J. Phys. Chem. Solids, Vol. 46, No. 3, pp 321-324 (1985).

22. Yokata, I., J. Phys. Soc. Japan 21, 420 (1966).

Ionic conductivity and activation energy (Ea) for a number of Li^+ based solid electrolytes

Solid Electrolyte	Form	σ at T°C (Ω^{-1} Cm^{-1})	Ea(eV)	T-range (°C)	Ref.
Li_3N	PC	2.0×10^{-4} at 25°C	0.16	25-180	(1)
Li_3N-LiI-LiOH	PC	1×10^{-3} at 25°C	0.21	50-300	(2)
Li-β-Al_2O_3	SC	1.3×10^{-4} at 25°C	0.16	150-180	(3)
(Li,Na)β-Al_2O_3	SC	1×10^{-3} at 25°C	-	-	(4)
LiI	PC	1×10^{-7} at 27°C	0.36	25-150	(5)
		$\sim 9 \times 10^{-4}$ at 285°C	0.92	250-350	(5)
$LiIH_2O$	PC	1.6×10^{-5} at 27°C	0.60	25-120	(6)
$LiI.2H_2O$	PC	2.0×10^{-6} at 50°C	3.67	40-70	(7)
$LiI.3H_2O$	PC	2.8×10^{-6} at 50°C	1.07	20-60	(7)
LiBr	PC	1.6×10^{-9} at 30°C	0.56	30-300	(8)
		$\times 10^{-5}$ at 350°C	-	350-500	(5)
LiCl	PC	1.7×10^{-7} at 182°C	0.42	182-375	(3)
		2.3×10^{-5} at 394°C	1.31	375-520	(3)
LiI-Al_2O_3 (40%)	DSES	1×10^{-4} at 27°C	0.40	50-30	(9)
		1×10^{-1} at 300°C	-	-	(9)
$LiI.H_2O.Al_2O_3$ (35%)	DSES	1×10^{-5} at 27°C	0.59	25-125	(10)

$Li_{14}Zn(GeO_4)_4$	PC	2×10^{-6} at 50°C	0.52	50-300	(11)
		1.25×10^{-2} at 300°C	-	-	(11)
Li_2WO_4 (α)	PC	1.43 at 700°C	0.36	575-860	(12)
Li_2SO_4 (β)	PC	2.5×10^{-6} at 300°C	1.09	280-470	(13)
		1.5×10^{-3} at 500°C	1.98	480-560	(14)
$LiCl.SiO_2$ (25%)	DSES	2.3×10^{-6} at 182°C	0.32	170-330	(3)
$LiCl.Al_2O_3$ (25%)	DSES	2.5×10^{-5} at 182°C	0.39	125-300	(3)
		6.9×10^{-4} at 394°C	0.51	300-440	(3)

(1) Boukamp and Huggins (1976), (2) Obayashi et al (1981a,b), (3) Whittingham and Huggins (1972), (4) Famington and Liang, (1977), (5) Ginnings and Phipps (1930), (6) Skarstad et al (1980), (7) Bishop et al (1966), (8) Haven (1950), (9) Liang et al (1978) (10) Pack et al (1979), (11) Von Alpen et al (1978), (12) Kvist and Lunden (1966), (13) Shahi (unpublished) (14) Kvist and Lunden (1965)